# Document made available under the Patent Cooperation Treaty (PCT)

International application number: PCT/US05/003090

International filing date: 21 January 2005 (21.01.2005)

Document type: Certified copy of priority document

Document details: Country/Office: US
Number: 60/538,765
Filing date: 23 January 2004 (23.01.2004)

Date of receipt at the International Bureau: 03 March 2005 (03.03.2005)

Remark: Priority document submitted or transmitted to the International Bureau in compliance with Rule 17.1(a) or (b)

World Intellectual Property Organization (WIPO) - Geneva, Switzerland
Organisation Mondiale de la Propriété Intellectuelle (OMPI) - Genève, Suisse

1288346

# THE UNITED STATES OF AMERICA

TO ALL TO WHOM THESE PRESENTS SHALL COME:

UNITED STATES DEPARTMENT OF COMMERCE

United States Patent and Trademark Office

*February 23, 2005*

**THIS IS TO CERTIFY THAT ANNEXED HERETO IS A TRUE COPY FROM THE RECORDS OF THE UNITED STATES PATENT AND TRADEMARK OFFICE OF THOSE PAPERS OF THE BELOW IDENTIFIED PATENT APPLICATION THAT MET THE REQUIREMENTS TO BE GRANTED A FILING DATE.**

**APPLICATION NUMBER:** *60/538,765*
**FILING DATE:** *January 23, 2004*
**RELATED PCT APPLICATION NUMBER:** *PCT/US05/03090*

Certified by

Jon W. Dudas

Under Secretary of Commerce
for Intellectual Property
and Director of the United States
Patent and Trademark Office

Attorney Docket No. US-5113-2P

Express Mail Label No. EL94205361US
Date of Deposit January 23, 2004

I hereby certify that this correspondence and the documents referred to a attached therein are being deposited with the United States Postal Service on the date set forth above, in an envelope as "Express Mail Post Office to Addressee" service under 37 CFR 1.10, Express Mailing Label Number as indicated above, addressed to Mail Stop Provisional Patent Application, Commissioner of Patents, PO Box 1450, Alexandria, VA 22313-1450.

By: Joann K. McCrea
Joann K. McCrea



**MAIL STOP PROVISIONAL PATENT APPLICATION**
**COMMISSIONER FOR PATENTS**
**PO Box 1450**
**Alexandria, VA 22313-1450**

Sir:

Transmitted herewith for filing is a provisional patent application under 37 CFR 1.53(c) of:

| Last Name | First Name | Middle Initial | Residence (City/State/Country) |
|---|---|---|---|
| FARIS | GREGORY | W. | MENLO PARK, CA, USA |
| KOTZ | KENNETH | T. | PALO ALTO, CA, USA |
| DEWHIRST | MARK | - | DURHAM, NC, USA |
| KALOGERAKIS | KONSTANTINOS | - | ATHERTON, CA, USA |
| AMIN | KHALID | - | SUNNYVALE, CA, USA |

Title: **"CANCEROUS TUMOR DETECTION USING OPTICAL VASCULAR FUNCTION "**

Enclosed are:

☒ 28 pages of the specification (including description)
☒ 10 sheet of drawings
☐ __ page Abstract
☒ A verified statement to establish small entity status under 37 CFR 1.9 and 37 CFR 1.27.
☒ The invention was made by or under a contract with the following agency of the United States Government: U.S. ARMY MEDICAL RSCH. ACQUISITION ACTIVITY under Government contract number DAMD17-02-1-0570.

Please charge Deposit Account No. 19-3883 as follows: (or check enclosed)
[ X ] Filing Fee $ 80.00 (small entity; $160 Large entity)
[ X ] Any additional fees associated with this paper or during the pendency of this application.

2 extra copies of this sheet are enclosed.

Respectfully submitted,

Correspondence Address:
**SRI INTERNATIONAL**
**333 Ravenswood Ave.**
**Menlo Park, CA 94025**

**Edward E. Davis**
Reg. No. 35,112
Applicant's Representative

Telephone: 650-859-2000
Facsimile: 650-859-6420

# U.S. PROVISIONAL PATENT APPLICATION

# CANCEROUS TUMOR DETECTION USING OPTICAL VASCULAR FUNCTION

By
Gregory W. Faris
Kenneth T. Kotz
Mark Dewhirst
Konstantinos Kalogerakis
Khalid Amin

Applicant
SRI INTERNATIONAL
333 Ravenswood Ave.
Menlo Park, CA 94025

# CANCEROUS TUMOR DETECTION USING OPTICAL VASCULAR FUNCTION

This invention was made with Government support under Grant DAMD17-02-1-0570 awarded by the U.S. ARMY MEDICAL RSCH. ACQUISITION ACTIVITY . The Government has certain rights in this invention.

## INTRODUCTION AND HYPOTHESES

The long-term goals of this research are to develop inexpensive technology to improve sensitivity and specificity (lower false-negative and false-positive rates) for early breast cancer detection and diagnosis. We believe that enhanced functional (physiological) optical imaging using a new type of contrast based on the unusual vascular function of tumors (atypical oxygenation improvement, atypical vasoactivity, and blood pooling) can meet these goals. Improved imaging through dense breasts (where X-ray mammography is less successful) is a secondary goal of this work. To our knowledge we are the only group investigating differential optical imaging using the vasoactivity of oxygen ($O_2$) and carbon dioxide ($CO_2$). We have been investigating this differential vasoactive optical imaging (DVOI) approach in animal model studies supported by an IDEA grant from the U.S. Army Breast Cancer Research Program. That work has demonstrated strong contrast between cancerous and noncancerous tissue during differential imaging in rodents in association with inhalation of $O_2/CO_2$ gas mixtures, providing proof-of-principle preliminary data in support of this TRC award application.

The contrast achieved by DVOI results from the vasculature in tumors and can arise from atypical oxygenation improvement, atypical vasoactivity, and blood pooling, as monitored by varying the levels of inspired $O_2$ and $CO_2$. We will use these differential vascular function measurements to augment the cancer-specific static contrast derived from elevated hemoglobin concentrations from angiogenesis and reduced local hemoglobin oxygenation from tumor hypoxia. A single imaging DVOI system can monitor both static and dynamic contrast mechanisms, thus providing the best possible sensitivity and specificity from an optical imaging system. $CO_2$ and $O_2$ are attractive contrast-enhancing agents because they are safe and require no injection or lengthy times between administration and imaging.

We hypothesize that the specificity of the differential contrast available with the DVOI approach will be sufficiently great to allow tumor detection with higher sensitivity, even at the poor spatial resolution available using optical imaging through the human breast. Other imaging techniques such as functional MRI (fMRI) or positron emission tomography (PET) are powerful imaging modalities, even with their low spatial resolutions. The strong contrast observed in our animal model studies and the finding that optical techniques can detect and locate picomole variations in chromophore concentrations over optical thicknesses comparable to those of the human breast[1] further supports this hypothesis.

## SPECIFIC AIMS

We have proven the capabilities of DVOI for detecting cancer in an animal model. We propose the translation of this work into the clinic to determine whether the DVOI approach is equally useful in humans. Our specific project aims are to:

(1) Modify and improve our DVOI system to allow human imaging.

(2) Perform clinical studies of DVOI mammography imaging on women scheduled for biopsies as a result of screening mammograms or suspicious lumps.

(3) Perform limited imaging on animal models to understand variability in the vasoactive response better and to test refinements in the imaging system, protocols, and data analysis.

(4) Modify and refine gas inhalation protocols for women by optimizing variations in gas composition and timing of gas inhalation to determine whether differential contrast can be further enhanced.

(5) Implement data analysis procedures to facilitate identification of significant image regions, to assist in understanding the large amount of data obtained in time-dependent two-dimensional (2-D) imaging, and to identify possible lesions for breast imaging.

## BACKGROUND AND SIGNIFICANCE

### Significance

Our objective is to test the capability of DVOI to meet the strong need for improved noninvasive imaging techniques for breast cancer detection. Improved imaging through dense breasts is a secondary goal of this work. Detecting cancer earlier and reducing false-negative results will improve clinical outcomes, and lowering the number of false-positive results will decrease the cost and physical and emotional trauma associated with unnecessary biopsies. X-ray mammography, the standard screening modality for breast cancer, is less effective at detecting cancer in younger women's breasts, which are denser than those of older women. Although the risk of carcinogenesis resulting from X-ray mammography is relatively low, concerns about risks of exposure over many years of screening are valid. For these reasons, other imaging techniques are being used and studied to augment X-ray mammography, including ultrasound, MRI, Tc-99m sestamibi scintimammography, optical techniques, and PET.

Optical techniques offer advantages for breast imaging, including functional imaging (imaging that provides information on tissue state and function), inexpensive instrumentation (our current imaging system costs less than $1,000 for parts), and no use of ionizing radiation. Optical imaging could prove useful as a secondary imaging modality to X-ray imaging for diagnosing, staging, or monitoring treatment of breast cancer. If DVOI proves successful, it could also find use as a primary screening modality. Because of its simplicity and low cost, DVOI can be efficiently incorporated into an X-ray or ultrasound imaging system[2] to provide functional information to complement the physical imaging of these modalities. DVOI may prove more effective in imaging dense breasts and may reduce or avoid the sometimes painful compression used for X-ray mammography.[3-6]

### Optical Breast Imaging

Optical imaging through the human body was one of the first modalities used for medical imaging, with early studies performed in the 19th century.[7-9] Optical imaging of the breast was reported in 1929.[10] Optical mammography was closely studied in the 1970s and 1980s,[11-13] although it proved inferior to X-ray mammography.[14,15] The primary problem with optical mammography is spatial resolution. Optical mammography has a spatial resolution of 0.5 to 1 cm, which means that blurring reduces contrast in smaller tumors. This limitation can be overcome by providing functional imaging information.

Interest in optical techniques for detecting breast cancer has increased , spurred by better understanding of light propagation through tissue,[16,17] time-resolved optical techniques for imaging[3,5,18-20] and quantifying tissue properties,[21,22] and new image reconstruction algorithms.[23-25] Industry (e.g., Carl Zeiss,[19] Phillips,[5] Seimens.[20]) has developed prototype imaging systems Applications of advanced optical mammography techniques have shown promising results.[2,4,6,19,26] A number of groups are examining the use of contrast agents for breast cancer detection.[26-30] Other useful optical imaging studies have incorporated window chambers.[31,32] A number of *ex vivo* studies of the optical properties of normal and diseased breast tissue have been performed.[33-35] Our studies complement these studies by investigating a new and promising method of increasing contrast.

**Functional Optical Imaging**

**Conventional imaging/static contrast.** Whereas X-ray imaging primarily provides structural information, optical spectroscopy imaging can provide information both on structure and tissue function. For example, optical measurements at different wavelengths can indicate total hemoglobin content and oxygenation—functional information that is significant for breast cancer detection. Tumor angiogenesis typically leads to elevated local hemoglobin concentrations.[4,6,36] In addition, tumors are often hypoxic, which can be observed optically as a decrease in hemoglobin oxygenation. Because tumors that are more hypoxic tend to be resistant to radiotherapy and chemotherapy and are more likely to be metastatic or invasive,[37-39] the degree of tumor hypoxia can be used to guide treatment. Tumor morphology also provides a source of contrast through variations in the optical scattering coefficient.[40] We propose to use the full range of available optical contrast by augmenting functional optical imaging using differential measurements related to tumor vascular function. We believe the broadest use of available contrast will be most effective for improving sensitivity and specificity.

**Differential vasoactive contrast** The atypical characteristics of vasculature produced through tumor angiogenesis[41,42] provide the basis for our DVOI approach. Blood vessels in tumors often exhibit distended capillaries with leaky walls and sluggish flow. These properties provide at least three types of contrast for optical imaging in conjunction with varying levels of inspired $O_2$ and $CO_2$. These types of contrasts are due to atypical oxygenation improvement, atypical vasoactivity, and blood pooling.[43-49] Dr. Britton Chance and collaborators have observed further evidence of compromised microvascular control through measurements of NADH (nicotinamide adenine dinucleotide) signals.[50] Because both $O_2$ and $CO_2$ are vasoactive, atypical tumor vasoactivity arising from administration of changing levels of these gases should provide strong imaging contrast. Tumor vessels are often contorted and leaky; thus, blood pooling in these vessels will delay response to oxygenation changes, providing another good contrast mechanism. Blood pooling itself can contribute to the atypical oxygenation improvement in tumors. However, as our preliminary studies have indicated, atypical oxygenation improvement persists beyond the transient response caused by blood pooling.

The unusual vasculature in tumors can be readily measured using functional optical imaging. For example, opposing vasodilation and vasoconstriction responses after 15% $CO_2$ and 85% $O_2$ (carbogen) inspiration are readily detectable by comparing hemoglobin content before and after carbogen is administered. Similarly, the changing response in tumor oxygenation after increased $O_2$ administration is easily measured by monitoring hemoglobin oxygenation levels before and after the $O_2$ level is increased. Changes associated with blood pooling are observable in delayed oxygenation changes

in the tumor. DVOI could also be combined with quantitative measurements of oxy- and deoxy-hemoglobin to improve overall sensitivity and specificity.

DVOI has a good potential for providing functional discrimination between benign and malignant lesions. Benign lesions tend to have rounded vasculature while malignant lesions tend to be more angular. Because the vasculature is different, it is likely that the vascular response to $O_2$ and $CO_2$ will also be different. If DVOI can provide information distinguishing benign and malignant lesions, this would be valuable.

There are additional motivations for examining differential contrast such as that associated with tumor vascular function. First, because the breast is highly heterogeneous, comprising the lobes (glandular tissue), fat, connective tissue, ducts, and supporting vasculature, using a broader palette of contrast mechanisms should provide more specificity for optical imaging and help compensate for that heterogeneity. Second, the more successful noninvasive optical measurements (e.g., pulse oximetry, functional brain imaging) are differential or dynamic. In pulse oximetry,[51,52] the differential signal of the cardiac pulse is combined with the optical signals of oxygenated and deoxygenated hemoglobin to derive blood oxygenation levels without detailed knowledge of the tissue type and level of scattering. For brain imaging,[53-56] differential measurements of hemoglobin or hemoglobin oxygenation are performed while the patient performs specific tasks such as finger tapping or is visual stimulated. As a result of the successes of these approaches, we will also combine dynamic and functional measurements for the studies proposed here. Finally, recent theoretical work has demonstrated improved results using dynamic or differential optical imaging techniques, both of which rely on changes in optical contrast over time.

## PRELIMINARY STUDIES

### Differential Vasoactive Imaging Studies

With support from the U.S. Army Breast Cancer Research Program, we are studying DVOI for mice and rats . Animal models allow us to monitor contrast for a range of tumor sizes and stages of development. Furthermore, the measurements are noninvasive and thus can be readily repeated on animals as our instrumentation and methods are refined. We perform measurements through tissue thicknesses similar to those of the human breast by partially immersing the anesthetized animals in liquid tissue phantoms that simulate the optical properties of breast tissue. Although this approach does not allow for the effects of tissue heterogeneity in the breast, it is the most practical method for studying contrast before beginning studies with human subjects.

We have constructed a continuous wave (CW) immersion imaging system to perform DVOI. Figure 1 provides a schematic of the instrument used for immersion imaging. The imaging system is composed of a near-infrared (NIR) light source, an immersion box, and a camera. The light source is made up of an array of bright light emitting diodes (LEDs) that emit NIR radiation with peak intensities at either 780 or 840 nm (Epitex L780-01AU and Epitex 840-01KSB, respectively). Switching between LED arrays enables measurements at different wavelengths and the determination of hemoglobin content and hemoglobin oxygenation.[57] This light source is directed at the sample immersion box, which contains the study animal in a heated (37°C), matching medium composed of water, ink, and Ropaque (Rohm and Haas Company). (Ropaque is made up of submicrometer polymer spheres used as an alternative to titanium dioxide in paints.) This immersion medium approximates the scattering and absorptive properties of the mouse tissue. The front of the immersion box is imaged onto the

camera. Images at each individual wavelength are then collected, digitized (8-bit resolution), and sent to the computer for analysis.

The compensation provided by immersing the animal in a tissue phantom improves image quality by removing changes in contrast associated with changes in tissue thickness and geometry, allowing better use of the dynamic range of the camera and providing more uniform illumination. When the match is good, the tissue almost disappears, and the image shows variations due to internal structure and contrast, which is what we want for *in vivo* imaging. The immersion medium serves to: (1) allow study of an effective tissue as thick as is typical for the human breast, and (2) enhance our measurements by eliminating the effects of boundaries. Although the tissue phantom lacks the heterogeneity of the human breast, there is considerable heterogeneity in the animal itself. Nonetheless, the effects of breast heterogeneity and human vasculature can be examined only in human studies, as proposed below.

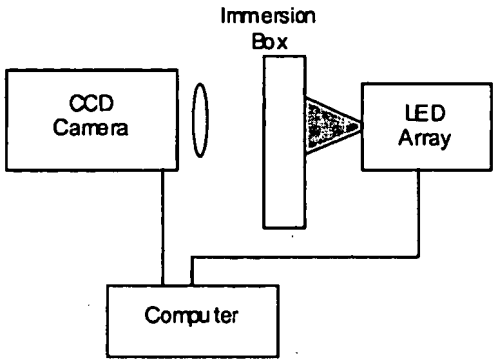


Figure 1. Schematic diagram of the CW immersion imaging system.

Tissue phantoms are prepared using our established methods.[22,58] An initial tissue phantom is prepared, an animal is immersed between the source and collection fibers, the changes in amplitude and phase are measured, and the phantom composition is adjusted according to the optical properties determined from the immersion measurement. This process is repeated until the optical properties of the immersion medium and the imaged tissue agree to within a few percent. The thickness of the tissue phantoms is varied by inserting Plexiglas sheets into the box containing the tissue phantom for the CW measurements.

We have compared three cameras for the CW imaging: a Dragonfly CCD (charge-coupled device) camera (Point Grey Research), a Pulnix TM-9701 CCD camera coupled to a Stanford Photonics Gen III image intensifier, and an ImagingSource DMK-3002-IR. The digital Dragonfly camera offers a significant improvement in signal-to-noise ratio (S/N) over other video cameras. Although the Dragonfly has a lower absolute sensitivity in the NIR region compared with the other video cameras, it has lower read noise and is capable of longer exposure times (>60 s), which will be important for imaging thicker tissue samples. We increased light throughput onto the imaging sensor by 20% by installing a large-aperture lens with high NIR transmission (JML Optics).

**Animal Models**

Human breast cancer cells (MDA 231) and mouse embryonic fibrosarcomas were grown in Dulbecco's minimum essential medium (DMEM) with glutamine and 10% fetal bovine serum. The cells were harvested when they were 80% confluent, using 0.25% trypsin. Cells were injected subcutaneously on the dorsum of the female athymic nude

mice (approximately 23 g, Harlan Laboratories). Both cell lines were used at a concentration of 2–3 million cells in 100 µl of DMEM for each animal. The tumor volumes were measured twice weekly.

**Animal Imaging**

Imaging experiments were conducted on animals with tumor volumes of 500–1000 $mm^3$. We used two-four animals for each experiment. After being anesthetized with 40 mg/kg of pentobarbital, the mice were secured to a 3-mm Plexiglas platform with black vinyl tape. Anesthesia was given in further doses of 20 mg/kg as needed to reduce stress associated with immersion and to keep the animal immobilized. Carbogen or air was administered to the immersed mouse via a nose cone at a flow rate of approximately 3 l/min. The optical path length of the immersion box was adjusted to match the thickness of the mouse (~2–2.5 cm). At this thickness, the exposure time of the camera allowed us to measure both wavelengths at approximately three frames per second. At the end of the experiment, the animals were sacrificed with an overdose of anesthetic agent.

Images of individual mice were recorded before, during, and after the administration of carbogen. Figure 2a shows one of these static images taken 134 s following the administration of the carbogen. The approximate outlines of both the mouse and the tumor have been placed on top of the image as a guide. The mouse's head is out of the immersion medium and is above the field of view in Figure 2. The hind legs and tail are seen at the bottom of the image. Figure 2b shows this same image after the subtraction of a background, which is simply an image of the mouse before the carbogen was turned on. Although the boundaries of the mouse and tumor are obscured by the good match with the immersion medium, it is clear from the difference image in Figure 2b that there are distinct regions of contrast between the tumor and the surrounding tissues of the mouse.

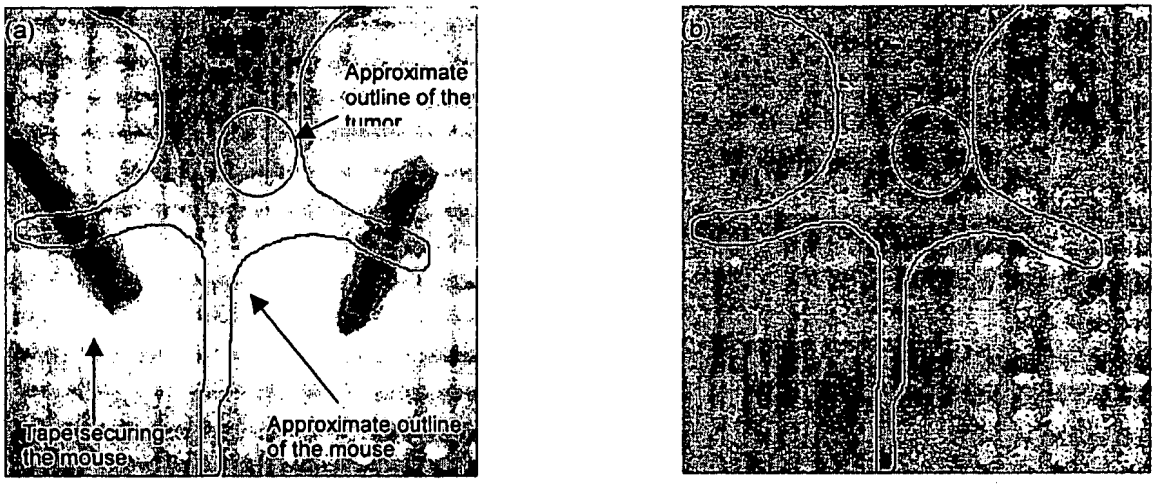


Figure 2. Images of mouse at 840 nm at 134 s after administration of carbogen;
(a) static image; (b) image from 2a with background subtracted.

**Temporal Variation in Differential Contrast**

The enhanced contrast between the tumor tissue and the mouse tissue due to the inhalation of the carbogen was monitored by averaging the changes in intensity over

areas within the difference images. Figures 3 and 4 show these averaged data for differences in the 780 nm and 840 nm images, respectively. The squares represent changes in the tumor tissue, the circles indicate an adjacent region within the mouse that does not contain the tumor, and the line represents the average of a part of the image not containing the mouse. The maximum change for both wavelengths is approximately ±10 units, and it is clear from the figures that distinct differences occur for the dynamics of the tumor tissue when compared with the normal mouse tissue. Furthermore, the background, which is a measure of lower limits for detection, varies just ±0.2 units.

Figures 3 and 4 indicate that several regions (e.g., near 55 s at 780 nm, and near 135 s at 840 nm) show strong contrast between tumor and surrounding tissue. Additional contrast is found after the carbogen is stopped; for 840 nm, the relative intensity of tumor and surrounding tissue reverses.

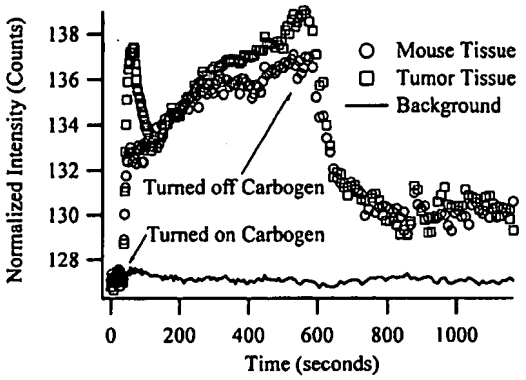


Figure 3. Temporal evolution of regions of the difference images at 780 nm.

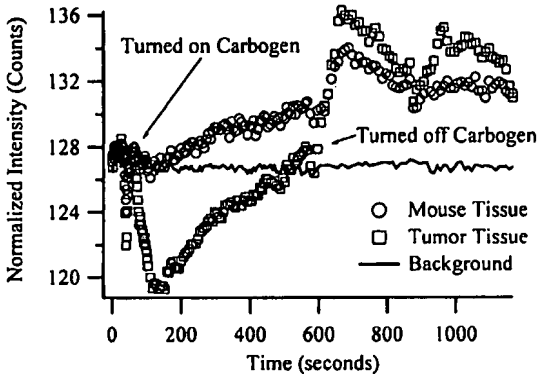


Figure 4. Temporal evolution of regions of the differ images at 840 nm

Although images at a single wavelength such as Figure 2b can be useful for cancer detection, it is also of interest to determine the changes in oxyhemoglobin and deoxyhemoglobin. We have analyzed the same image data set used to produce Figures 3 and 4 to calculate approximate path-integrated oxyhemoglobin and deoxyhemoglobin. The absorption at 780 nm and 840 nm can be described as:

$$\mu_a^{\lambda} = 2.3\left\{\varepsilon_{Hb}^{\lambda}[Hb] + \varepsilon_{HbO_2}^{\lambda}[HbO_2]\right\}$$

where $\lambda$ is the wavelength of interest, [*Hb*] and [$HbO_2$] are the concentrations (moles/L) of deoxygenated and oxygenated hemoglobin, respectively, and $\varepsilon$ is the molar absorption coefficient.[59] Using Beer's Law, we can describe the change in the absorption coefficient $\mu_a$, at time *t* after a baseline image has been taken as:

$$\Delta\mu_a^{\lambda} = \mu_a^{\lambda,t} - \mu_a^{\lambda,baseline} = 2.3\log_{10}\left[\frac{I_{baseline}}{I_t}\right]/l$$

where *I* is the intensity of transmitted light and *l* is the pathlength in cm, corrected appropriately for the differential pathlength factor for the animal tissue.[60,61] We can obtain a rough measure of the change in path-integrated oxyhemoglobin and deoxyhemoglobin concentrations by assuming that the differential pathlength factor is the same at both wavelengths. By manipulating equations (1) and (2), we see that:

$$\begin{pmatrix} \Delta\mu_a^{780} \\ \Delta\mu_a^{840} \end{pmatrix} = \frac{2.3}{l} * \begin{bmatrix} \varepsilon_{Hb}^{780} & \varepsilon_{Hb_{O_2}}^{780} \\ \varepsilon_{Hb}^{840} & \varepsilon_{Hb_{O_2}}^{840} \end{bmatrix} \begin{pmatrix} \Delta[Hb] \\ \Delta[HbO_2] \end{pmatrix}$$

Because of the finite bandwidth of the LEDs, we calculated the absorption coefficient by integrating the wavelength-dependent absorption coefficient with the normalized spectra of the LEDs for each wavelength respectively:

$$\varepsilon^i = \int \varepsilon(\lambda) I^i(\lambda) d\lambda$$

This led to the following equations for the concentrations of *Hb*, $HbO_2$, $Hb_{total}$ at time *t*:

$$\Delta[Hb](t) = 2.3 * \left( 7.507 * 10^{-4} * \log_{10} \frac{I_{\beta}^{780}}{I_{\iota}^{780}} - 5.271 * 10^{-4} * \log_{10} \frac{I_{\beta}^{840}}{I_{\iota}^{840}} \right) / l,$$

$$\Delta[HbO_2](t) = 2.3 * \left( -5.255 * 10^{-4} * \log_{10} \frac{I_{\beta}^{780}}{I_{\iota}^{780}} + 7.996 * 10^{-4} * \log_{10} \frac{I_{\beta}^{840}}{I_{\iota}^{840}} \right) / l,$$

$$\Delta[Hbtot](t) = \Delta[Hb](t) + \Delta[HbO_2](t)$$

We used these calculations to calculate the approximate temporal variation of the total hemoglobin, oxyhemoglobin, and deoxyhemoglobin shown in Figure 5. These values were in turn used to calculate the approximate change in $O_2$ content (oxyhemoglobin change, minus deoxyhemoglobin change) shown in **Error! Reference source not found.**. Several observations arise from these images: The tumor vasculature shows more erratic behavior, as seen from the oscillations at the beginning of carbogen inhalation. the failure to return to baseline for the total hemoglobin concentration (Figure 5), and the overshoot in $O_2$ content at the end of the carbogen inhalation (**Error! Reference source not found.**). The magnitude in changes of oxyhemoglobin and deoxyhemoglobin are accentuated in the tumor (Figure 5). The increase in $O_2$ content of the tumor is delayed relative to the rest of the animal (Figure 5 middle and **Error! Reference source not found.**), which may be due to blood pooling in the tumor.

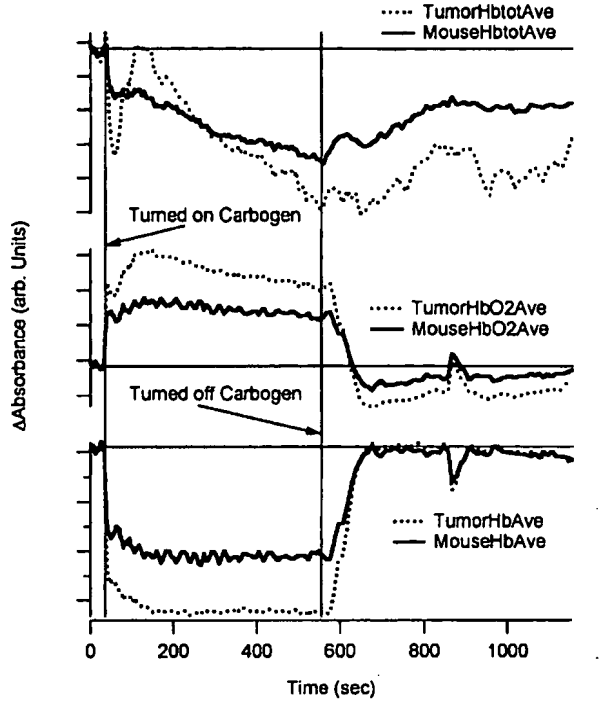


Figure 5. Temporal variation of relative changes in total hemoglobin (top), oxyhemoglobin (middle), and deoxyhemoglobin (bottom) during carbogen inhalation. The tumor region is shown by the dashed line; the region on the mouse torso away from tumor is shown by the solid line.

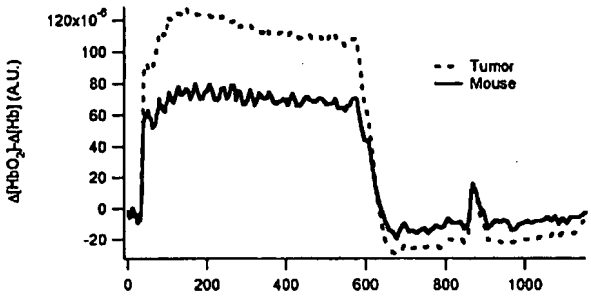


Figure 6. Temporal variation of relative changes in total $O_2$ content (oxyhemoglobin change, minus deoxyhemoglobin change) during carbogen inhalation. The tumor region is shown by the dashed line; the region on the mouse torso away from tumor is shown by the solid line.

The same processing used for Figures 5 and 6 can be used to produce images representing approximate path-integrated oxyhemoglobin and deoxyhemoglobin (Figure 7). These differential vasoactive images show a dramatic increase in tumor contrast as compared with a raw or static image (Figure 2).

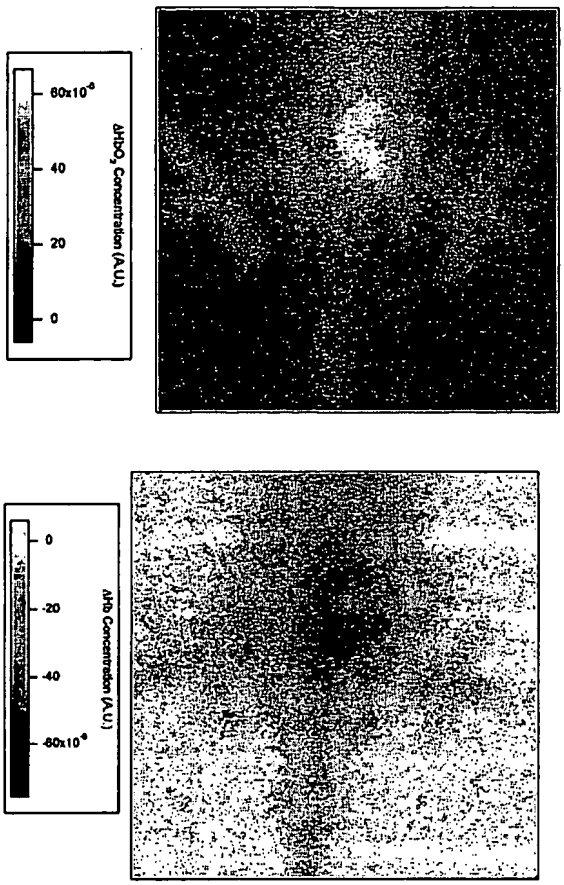


Figure 7. Relative concentrations of oxyhemoglobin (left) and deoxyhemoglobin (right) concentrations at 140 s (100 s after carbogen administration).

**Principal Component Analysis**

The imaging experiments described above generated large sets of data. Typically, images with $10^5$ pixels at two wavelengths are recorded every 2–10 seconds over the cycling period of carbogen administration (approximately 10 to 20 minutes). From our preliminary studies with this method, we expect to see <7% change in image intensity following carbogen administration. Because extracting such small signal changes from large data sets poses a formidable challenge, researchers have developed techniques that generate smaller sets of orthogonal images to describe the generated data.[62,63] In practice, these methods have been shown to accurately describe data sets of 10,000 images with only ~100 eigen images.[64]

In the most basic adaptation of these methods, known as principal component analysis (PCA), the set of recorded images is represented by:[62,63]

$$f = f(t, \mathbf{x})$$

where ***x*** describes the spatial pixel grayscale values of the image, and *t* is the time at which the image data was collected. Researchers have shown that these images, *f(t,**x**)*, can be decomposed into the set of orthogonal functions $a_n(t)$ and $\varphi_n(\mathbf{x})$ by:

$$f(t,\mathbf{x}) = \sum_n \mu_n a_n(t)\varphi_n(\mathbf{x}).$$

A series of *T* time images containing P pixels can be described by the matrix:

$$\mathbf{M} = \begin{bmatrix} f(1,1) & f(1,2) & \cdots & f(1,P) \\ f(2,1) & f(2,2) & \cdots & f(2,P) \\ \vdots & & & \vdots \\ f(T,1) & \cdots & \cdots & f(T,P) \end{bmatrix}$$

This matrix can then be decomposed into the different $a_n(t)$ and $\varphi_n(\mathbf{x})$ components through the general technique of singular value decomposition:

$$\mathbf{A}_n = \begin{bmatrix} a_n(1) \\ \vdots \\ a_n(T) \end{bmatrix}, \mathbf{V}_n = \begin{bmatrix} \varphi_n(1) \\ \vdots \\ \varphi_n(P) \end{bmatrix}, \text{and } \mathbf{U} = \begin{bmatrix} \mu_1 & & 0 \\ & \ddots & \\ 0 & & \mu_T \end{bmatrix}$$

and

$$\mathbf{M}=\mathbf{AUV}^\dagger$$

The columns of **V** contain the orthonormal spatial basis functions, the orthonormal columns of **A** describe the time-dependence of the spatial basis functions, and **U** contains the weighting factors for the two matrixes **A** and **V**. We have applied this simplified PCA method to our data as a first step toward simplifying the extraction of spatial images.

As a first step in processing the data, we followed this procedure to determine changes in oxyhemoglobin and deoxyhemoglobin, scaled by some pathlength factor *l* as described above. The time-dependent images that describe $\Delta[Hb]$ and $\Delta[HbO_2]$ were ordered into a matrix as shown in equation (10), and the singular value decomposition was carried out to obtain the matrices **A**, **U**, and **V**. Figure 8 presents a plot of the normalized scaling factors contained along the diagonal of U. Only the first three or four eigen images contribute significantly to the set of images that describe the hemoglobin dynamics in our study.

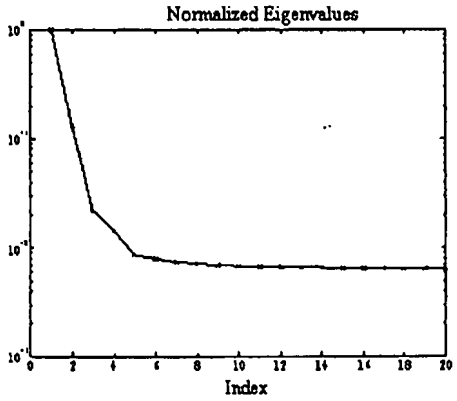


Figure 8. Normalized eigen value spectrum.

Figure 9 shows the first two eigen images corresponding to the first two columns of matrix **V**. The contrast between the tumor and the surrounding tissue is evident in the second image. The time-dependent weighting of the second eigen image in the $\Delta[Hb](t)$ and $\Delta[HbO_2](t)$ sets of images can be determined from the matrix product of **A**•**U**, and is shown in Figure 10.

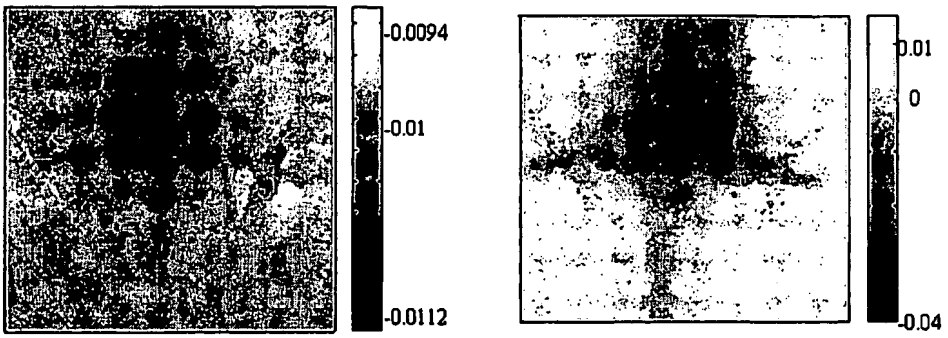


Figure 9. First two eigen images from principal component analysis.

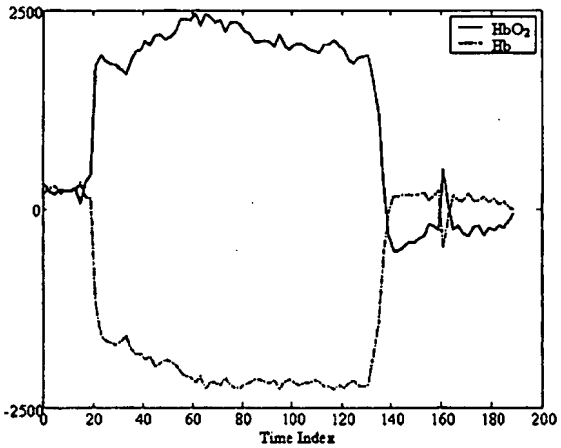


Figure 10. Temporal variation of the eigen image scaling factor.

**Remaining Project Goals**

Our U.S. Army Breast Cancer Research Program IDEA award ends in early May 2004. The primary unfinished goal of this project is the comparison of differential contrast with static contrast. In the remaining 5 months of this project, we will be performing frequency domain measurements to examine static contrast. These measurements will be performed using an existing homodyne frequency domain system. Source and detector fibers will be scanned in the immersion medium to enable quantification of the static contrast and provide semiquantitative results from the differential measurements.

**Methods for Improving Quantification (possible future work following proposed project)**

Dr. Faris has extensive experience with the frequency domain technique,[22,58,65-73] a method used to improve the quantification of tissue properties, and has more than 15 years of experience with optical tomography instrumentation[65,74-79] and algorithms.[80] This experience could prove useful in enhancements of this technique at some future date, if necessary.

## RESEARCH DESIGN AND METHODS

### Aim 1. Enhance Imaging System

We will modify our existing imaging system to improve its performance by: adding another wavelength to enhance the imaging of water, increasing the illumination power, and increasing camera sensitivity. These modifications will enable us to image through large tissue phantoms with S/Ns limited only by shot noise, which is a fundamental limitation for any imaging process. High S/Ns can be very effective for differential imaging because image heterogeneity is removed during the image subtraction process. That is, subtraction of two images taken of the same field of view yields an image of zero intensity if nothing has changed.

Water concentrations are known to influence measurements of hemoglobin.[81] Thus, performing imaging at a wavelength dominated by water absorption may assist in quantifying oxyhemoglobin and deoxyhemoglobin measurements. Because of the high fraction of water in blood, images with dominant water absorption may also help monitor blood volume directly. Although the change in water content associated with vasodilation or vasoconstriction is relatively small, we have found that the differential imaging is quite sensitive to such changes. Thus, we may be able to monitor changes in blood volume directly using differential images at 970 nm, a wavelength dominated by water absorption. Observations that vasoconstriction may lead to changes in hematocrit[82] may mean that a water-based measurement of blood volume can also provide information on blood plasma changes, which are somewhat different from the changes provided by hemoglobin measurements. Measuring blood plasma changes may prove to be infeasible, but attempting this approach is worthwhile. Monitoring blood volume changes with water absorption is not critical to the success of our imaging approach, but it has the potential to make the overall imaging approach more powerful if it works.

We will increase the power available from our LED array. The images in the Preliminary Studies section were obtained using 21 LEDs at each wavelength. We will increase the power by a factor of 20 by using more LEDs and increasing their brightness by operating them at higher drive currents. We have shown in burn-in tests that the LEDs can be operated significantly above their typical operating currents for many weeks without incurring problems. The LEDs are turned on for only short periods during imaging at each wavelength, thereby increasing the practicality of higher current operation without LED damage.

We will substitute a more sensitive camera for the one cited in the Preliminary Studies section. We will purchase a Retiga 1350 EX camera produced by Q-Imaging. This CCD camera is approximately 2 times more sensitive in the NIR than our current camera. In addition, the camera-sensitive area is 4 times larger. These two improvements will lead to an overall enhancement in camera sensitivity of roughly a factor of 8. In combination, the increased illumination and more sensitive camera should improve overall system sensitivity by more than 100 times.

### Aim 2. Perform Human Studies

We will perform optical imaging on human subjects to test the approach. These studies will be performed at the Stanford University Medical Center (approximately 2 miles from SRI) under the overall supervision of Dr. Birdwell, Associate Professor of Radiology. Dr. Birdwell's assistant will be responsible for recruiting volunteers, maintaining records, and coordinating scheduling. The imaging system will be operated by a postdoctoral associate from SRI. To provide the patients being imaged with a greater sense of ease with the imaging process, the postdoctoral associate will be a

woman. This imaging may be performed in either the stereotactic biopsy room or the ultrasound-guided biopsy room at Stanford.

Subjects will be recruited from women referred for biopsy, either on the basis of screening or on the presence of a suspicious lump. Optical imaging will be performed before the biopsy to avoid any influence the biopsy procedure might have on imaging measurement and interpretation. The imaging will be performed using only one or two inhalation protocols so that the total imaging takes only a few minutes. Imaging will cease if the patient feels uncomfortable or wishes to stop for any other reason. Imaging will be performed on 10 subjects in the first year and 15 patients in the second and third years, for a total of 40 patients. If the sensitivity and specificity are high, measurements on this number will enable us to calculate 95% confidence intervals for specificity and sensitivity with a half-width of approximately 15%. Volunteers for the imaging will be given a remuneration of $50.

Different imaging methods may be used for differential vasoactive imaging of the breast. The imaging may be performed with or without compression and with or without immersion. We hypothesize that optimal imaging will entail using at least mild compression and immersion. Compression would be advantageous for two reasons: first, with compression the total imaging distance is less, leading to a higher S/N, and hence increasing the likelihood of detecting a smaller tumor. Second, X-ray mammography uses compression. We believe that combining optical imaging with X-ray imaging would provide a powerful method—given their low-cost and the possibility that both imaging techniques could be performed simultaneously. In fact, with the transition to digital mammography using semiconductor-based cameras, the imaging could share the same detector. That combination would lead to an improvement in sensitivity and specificity over either modality alone. Achieving this improvement would require coregistration of images from the two modalities, which could be achieved most practically if compression were used for each imaging method.

From our experience with the animal imaging described in the Preliminary Studies section and other *in vivo* imaging,[83] we believe that the sensitivity of the imaging will be highest when immersion is used. With immersion, all portions of the breast are imaged, with nearly the same illumination reaching the detector and providing more optimal use of the dynamic range of the camera. That is, the entire image may be acquired with a high level of illumination, and hence high S/N. For the nonimmersed breast, variations in the transmitted light intensity across the breast will be large. To avoid camera saturation in the thinnest regions, low light levels will be obtained in the thicker regions. Thus, the thicker regions will have a lower S/N, and worse imaging results. Researchers have used the phase measurement available with frequency domain measurements to perform correction for edge effects.[84] Immersion achieves a similar goal.

Immersion can be achieved in two ways: first, the patient lies prone on a table similar to a stereotactic breast biopsy table with the breast immersed in a matching medium below.[5,85] A second approach is to surround the breast with a doughnut-shaped transparent bag containing a tissue phantom liquid. The bag would be filled to a slight overpressure to press against the breast in a manner similar to a blood pressure cuff, except that the overpressure would be much less. This method would achieve the same advantage of immersion but with less preparation and cleanup required. We plan to use the second immersion method. If we find significant problems, we will use the method with the breast pendant in the matching medium. For immersion-based imaging, a new bag with fresh immersion medium will be used for each patient. The immersion medium will be maintained at 37°C.

Imaging will be performed only on patients who already have suspicious lesions. However, optical imaging could identify another suspicious breast region that is not identified by the imaging modality being used for the biopsy (X-ray or ultrasound). Because the diagnostic capability of the optical imaging is still unproven, further imaging of a lesion identified only by optical imaging will not be covered by the patient's medical insurance. To address this eventuality, the budget includes the cost for MRI for follow-up on lesions seen only with optical imaging. If MRI does not detect the lesion that has been detected optically, the patient will be scheduled for a follow-up examination after 6 months.

The relative sensitivity and specificity of a diagnostic method depend on the criteria used. Relevant criteria include percentage change in hemoglobin content and hemoglobin oxygenation, and the relative signs (i.e., did each increase or decrease). As with any diagnostic method, by varying the criteria used either sensitivity or specificity can be made high, but at the expense of the other dimension. To assist in the analysis of the data, we will use a receiver operating characteristic (ROC) curve, which plots sensitivity versus false positive fraction; the free parameter is the criterion or threshold used for diagnosis. The area under the ROC curve gives a measure of the quality of the method; an area near 1 is desirable. We will prepare ROC curves for each contrast mechanism and for the contrast mechanisms in conjunction.

To test the null hypothesis of no association between optical mammography results and biopsy status, we will perform a sign test, wherein a correct prediction (i.e., a patient with agreement between the optical mammography and biopsy results) is coded as a 1 and an incorrect prediction is coded as a 0. Under the null hypothesis (and conditional on observing 8 patients with cancers as determined by biopsies), the number of correct predictions follows a distribution that is the combination of a Binomial(8, 0.2) and a Binomial(32, 0.8) distribution (i.e., 8 flips of a coin with a probability of 20% of being correct and 32 flips of a coin with a probability of 80% of being correct). Under the conservative alternative hypothesis, the number of correct predictions follows a distribution that is the combination of a Binomial(8, 0.8) + Binomial(32, 0.8) = Binomial(40, 0.8) distribution (that is, 40 flips of a coin with a probability of 80% of being correct).

We reject the null hypothesis if we obtain more correct predictions than we would expect under the null hypothesis (i.e., the number of correct predictions exceeds the 95-th percentile of the distribution under the null hypothesis). Monte Carlo simulation (1000 trials) shows that the 95-th percentile of the distribution under the null hypothesis is 32 (i.e., there is only a 4.3% probability that under the null hypothesis there will be 32 or more correct predictions). Consequently we reject the null hypothesis if we find 32 or more correct predictions. Monte Carlo simulation (1000 trials) under the conservative alternative hypothesis shows that there is a 60% probability of observing 32 or more correct predictions. Therefore, the power is 60% under the conservative hypothesis. If the results in humans are as good as the results in animals, then our specificity and sensitivity will each be approximately 90%. Under this alternative hypothesis, the power of the study is approximately 98% (i.e., there is a 98% probability that we will find 32 or more correct predictions out of 40 patients).

**Aim 3. Perform Animal Model Studies**

We will supplement our human studies with limited animal model studies to achieve better understanding of findings for humans, of differences between animals and humans, and of variation between tumor types. Work with animals will also help minimize inconvenience to subjects and will allow greater flexibility. For example, we

can perform studies over a longer period, perform more measurements in a single day, more readily repeat measurements on different days, compare results with identical cancer types in different animals, compare results on different cancer types, and measure small tumor sizes.

We will perform imaging in a number of additional animal cancer models to improve our understanding of the range of response possible with vasoactive differential imaging. Understanding how the response differs among tumor types will enable us to adapt the image interpretation appropriately. Ideally, each different tumor type or stage of tumor growth will display sufficiently reliable characteristics to allow tentative identification of tumor type or assist in cancer staging. The animal model will help us reproduce results found in the human studies and to vary those results.

Animal imaging will also allow us to refine our instrumentation and data analysis. We can perform measurements on the same animal at different times during tumor development or use different gas inhalation protocols. This work will enhance our ability to understand how the imaging signatures change during tumor development and how different gas inhalation protocols change the imaging response for the same tumor and animal.

We have experience with a number of breast cancer models for this animal model work. To gain a greater sense of the variability of the differential vasoactive response, we will compare an orthotopic model with various ectopic tumors (both syngeneic and xenograft) and orthotopic tumors in lactating rats. Comparison of the rat orthotopic model with measurements on ectopic mouse tumors will provide a good sense of the variability of the differential vasoactive response. We will perform contrast measurements on three rat models (orthotopic mammary tumors, orthotopic mammary tumors in lactating mammary glands, and ectopic mammary tumors) and three mouse models (4T1, MCF-7, and MDA-231). We will use a total of 30 rats and 30 mice to obtain modest confidence intervals for our preliminary studies (about 15%).

**Rat Orthotopic Breast Cancer Model**

To construct a cancer tumor model that gives representative results with improved reliability, we will use orthotopic tumors with the syngeneic mammary adenocarcinoma R3230.[86,87] Orthotopic tumors are considered to be more similar to human mammary carcinomas in regard to histology and structure than ectopic tumors because they are grown in the site of origin (i.e., the mammary gland). In addition, the makeup of the mammary gland—a collection of inactive lobular glands with abundant stroma and fat tissue—is quite similar across different species. Accordingly, we will use syngeneic orthotopic mammary adenocarcinoma R3230 in female Fisher 344 rats. We will inject 5 million cells into the subcutaneous tissue of the thigh. Once the donor tumor reaches a volume of 400–600 $mm^3$, the tumor will be surgically removed. We will surgically implant 1-$mm^3$ tumor pieces from the donor tumor into the mammary fat pad of recipient female F344 rats. We will use one distal mammary gland on the mammary line and use the other glands as controls.

**Orthotopic Mammary Tumors in Lactating Mammary Gland**

We will use lactating mammary glands as one of the sources of normal tissue for comparison of the tumor results. The multifold enhancement of the blood supply in the lactating mammary gland will challenge the ability of the imaging approach to distinguish normal and cancerous tissue. Lactation signifies the most active state of the mammary gland because the blood supply is enhanced multiple times to supply functional glands that are secreting milk. As a result, imaging is much more difficult because of the extensive noise induced by that activity inside the mammary gland, especially if a

growing tumor is present. We will use pregnant female Fisher rats for these experiments. With surgical implantation of 1-$mm^3$ tumor pieces from the donor tumor, tumor growth will proceed at a rapid rate. This is important because lactation will continue for no more than 3 to 4 weeks postpartum. Only one gland will be selected for the tumor injection, with the other glands used as controls.

**Ectopic Tumors**

We will also study ectopic tumors using the same cancer cell line. Study findings will provide information on the relative roles of the cancer cell line and of the tumor site on the nature of the vasoactive imaging. For the ectopic model, we will surgically implant tumor pieces approximately 1 $mm^3$ in size subcutaneously into the thighs of Fisher 344 rats.

**Mouse Mammary Carcinoma 4T1 Cell Line**

The 4T1 cell line[114,115] is a very aggressive metastatic mouse mammary cancer cell line. The tumors will be generated through cell injection of 1 million cells in subcutaneous tissue of the thigh region of the female Balb/c mouse. The tumor volume will be measured twice weekly. The imaging will be carried out in tumors having volumes ranging from 200-800 $mm^3$.

**Human Cancer Cell Lines-Xenografts**

We will use two commonly used human breast cancer cell lines, MCF-7[116,117] and MDA-231,[118] to generate orthotopic (mammary fat pad) tumors in nude mice. Since MCF-7 is an estrogen-dependent cell line, the animals will also be injected with an estrogen pellet over the dorsum. The tumor volume will be measured twice weekly. The imaging will be carried out in tumors having volumes ranging from 200-800 $mm^3$.

**Animal Care and Handling**

The SRI animal research facility is AAALAC-accredited. The temperature is maintained at 72 ± 5°F, with relative humidity at 35—70% and a 12-h light/dark cycle. Rodents have certified Purina rodent chow and drinking water freely available. The source water is recirculated, deionized, UV-treated, and 5-μm filtered. It is analyzed quarterly for metals and trace contaminants.

Each rat will be sacrificed following imaging and before undue pain from the tumor occurs. Rodents will be sacrificed by AVMA-approved euthanasia solutions (i.e., sodium pentobarbital [200 mg/kg I.P.] or Buthanasia [150 mg/kg I.P.]). If tumor volumes reach ≥ 1,000 $mm^3$ or if weight loss exceeds 20%, rats will be sacrificed regardless of whether the planned imaging is complete.

**Animal Imaging**

Animals will be anesthetized with sodium pentobarbital (40 mg/kg I.P.) before imaging to minimize trauma and to facilitate performance of the imaging. Imaging will be performed using a method similar to that used for the preliminary studies. The anesthetized animals will be taped to a plastic paddle and immersed in the tissue phantom, which will be maintained at 37°C. It is known that anesthetization can cause physiological changes[88] that might affect our imaging measurements; this is especially the case for the ketamine/xylazine combination, which we have not opted to use. However, changes associated with sodium pentobarbital are expected to be fewer than the physiological changes associated with an animal under stress from constraint.

The animals will be monitored regularly and the tumor volume measured twice weekly. We will carry out optical imaging at three time points corresponding to different tumor sizes (200 $mm^3$, 500 $mm^3$ and 1000 $mm^3$). The animals will be anesthetized with

35-45 mg/kg of pentobarbital before the start of the imaging procedure. After the imaging session, the tumors will be removed and fixed in 10% formalin. Histological analyses will be carried out on H&E (hematoxylin and eosin) stained slides. We will conduct semiquantitative observations of certain well-defined morphological changes that occur as the mammary carcinoma grows, such as necrosis, cystic changes, and development of solid areas, and compare them with the optical imaging results. Such changes should be observable optically. Necrosis and cystic changes should both have low hemoglobin levels, compared with an actively growing tumor, and so be clearly identifiable.

**Data Analysis**

The measured properties for tumors will be compared with those of neighboring tissue and lactating mammary glands in the animals. To verify the anatomy observed in the images, tissues from rats will be embedded in paraffin and processed for pathological examination. We will carry out hematoxylin and eosin stain for general histology and immunohistochemistry for blood vessel identification to gain an understanding of the results from optical imaging and actual tumor morphology at the last imaging session. The nature of the tumor vasculature from the pathology will be compared with the imaging results to determine how it contributes to the images obtained. This information will be helpful in continuing development of this imaging approach. Drs. Amin, Haroon, and Dewhirst will provide advice on cancer biology relevant to the images. Dr. Amin is at SRI and will be performing the animal model work. Dr. Haroon, a consultant for this project, has experience with the proposed animal models and the role of hypoxia in cancer. His offices are near SRI, and he is readily available for consultations. Dr. Dewhirst, also a consultant, will provide additional expertise on the role of $O_2$ transport in tumors. He is performing related research using MRI instead of optical imaging.

**Aim 4. Study Gas Protocols**

We will examine other protocols for gas inhalation. Measurements will be performed with varying inhalation gas composition and administration time. Gas mixtures will be produced on demand using computer-controlled gas flow controllers. Three gases will be used to produce these mixtures: nitrogen, $O_2$, and $CO_2$. In this way we can rapidly alternate among gas compositions, continuously varying the levels of $CO_2$ and $O_2$ in a nitrogen buffer, or create carbogen. These studies are of interest because $CO_2$ and $O_2$ have opposing effects on vasculature (vasodilation versus vasoconstriction, respectively). Using these two mechanisms in opposition or in alternation should produce potentially useful results from the differential vasoactive imaging. For example, elevated $CO_2$ levels may be administered for a period of a minute, followed rapidly by a period of elevated $O_2$. The same protocol could be repeated with a small overlap between the elevated $CO_2$ and $O_2$ levels. With the computer-controlled flow controllers, we can sequentially administer different gas mixtures to the same individual, taking care that the vasculature recovers sufficiently between the changes. We expect that these studies will result in more effective discrimination between cancerous and noncancerous tissue, and perhaps provide means of distinguishing among different tumor types.

We will perform studies of gas inhalation protocols on both animals and humans. With animals, we can perform studies over a longer period, conduct more measurements in a single day, more readily repeat measurements on different days, compare results with identical cancer types in different animals, and measure small tumor sizes. The protocols are likely to be different for humans because of the different respiratory rate, heart rate, size, and the fact that the animals are anesthetized and the humans are not.

Animal studies will be performed on different animal cancer cell lines to determine whether we can distinguish among those lines. If we find certain protocols accentuate the difference among cell lines or animals, we will modify that protocol to see whether the degree of discrimination can be increased. If certain protocols reduce discrimination, we will modify those protocols to determine whether the degree of discrimination can be decreased while still maintaining the discrimination between cancerous and noncancerous tissue. Protocols with and without strong discrimination are both likely to be of clinical value. Protocols that do not discriminate strongly among tumor types may prove more useful for imaging related to screening, when the primary interest is cancer detection. Protocols with stronger discrimination among different tumor types might be used when suspicious lesions are detected. The more promising gas protocols found for the animals will be used in the clinical studies, provided that the gas compositions remain within safe levels for humans.

**Aim 5. Develop Image Analysis Tools**

The measurements acquired for differential vasoactive imaging comprise three-dimensional (3-D) datasets as illustrated in Figure 11. The two spatial dimensions and one temporal dimension differ from other 3-D imaging modalities such as MRI or computed tomography (CT), which have three spatial dimensions. For those imaging modalities, visualization tools often create 2-D images as cross sections through the 3-D data set. Regions of interest can be probed by changing the orientation of the cross section. This same approach is also used for ultrasound imaging, where the ultrasound technician achieves different sections in real time by changing the orientation of the ultrasound probe.

Visualization of data such as in Figure 11 can be performed by taking cross sections at different orientations. In fact Figure 2 and Figures 3 and 4 are examples of a cross section and a line section through such a data set at constant time and position, respectively. However, both the spatial pattern (such as Figure 2b) and the temporal pattern (such as Figure 3) are necessary to define features in this data set. Simultaneously capturing both of these features requires a different sort of image analysis tool. One such tool is PCA.

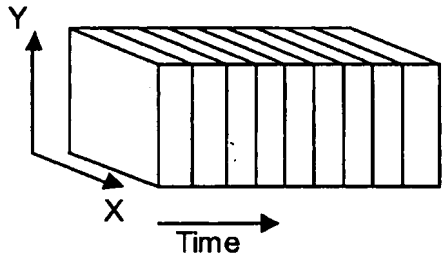


Figure 11. Form of 3-D data for differential vasoactive imaging.

We will apply PCA similar to that described in the Preliminary Studies section. We will adapt the approach to allow automated data processing of temporal image data sets of oxyhemoglobin, deoxyhemoglobin, and total hemoglobin, and change in $O_2$ content. To improve the results, we will study methods such as spatial and temporal averaging conditioned on the image features and the use of *a priori* information such as the temporal profile of the gas inhalation protocol. For breast imaging, we expect the

number of eigen images may be larger. We will study methods for classifying the eigen images (e.g., by tumor type, other feature such as blood vessels).

**Future Work**

Following this TRC project we will have a very good indication of whether DVOI is effective for breast cancer detection. If the technique shows good sensitivity and specificity, we plan to continue clinical development of the approach. Depending on the outcome of the human studies, this future work may involve further imaging system refinements, human studies with larger numbers of subjects, human studies targeted at specific imaging needs such as screening young women with known propensity for developing breast cancer, or development of a combined imaging modality such as optical and x-ray imaging.

## REFERENCES


1. B. Chance, K. Kang, L. He, J. Weng, and E. Sevick, "Highly sensitive object location in tissue models with linear in-phase and anti-phase multi-element optical arrays in one and two dimensions," Proc. Natl. Acad. Sci. U. S. A. **90**, 3423-3427 (1993).
2. Q. Zhu, E. Conant, and B. Chance, "Optical imaging as an adjunct to ultrasound in differentiating benign from malignant lesions," Proc. SPIE **3597**, 532-539 (1999).
3. T. O. McBride, B. W. Pogue, E. D. Gerety, S. B. Poplack, U. L. Österberg, and K. D. Paulsen, "Spectroscopic diffuse optical tomography for the quantitative assessment of hemoglobin concentration and oxygen saturation in breast tissue," Appl. Opt. **38**, 5480-5490 (1999).
4. J. B. Fishkin, O. Coquoz, E. R. Anderson, M. Brenner, and B. J. Tromberg, "Frequency-domain photon migration measurements of normal and malignant tissue optical properties in a human subject," Appl. Opt. **36**, 10-20 (1997).
5. S. B. Colak, D. G. Papaioannou, G. W. 't Hooft, M. B. van der Mark, H. Schomberg, J. C. J. Paasschens, J. B. M. Melissen, and N. A. A. J. van Asten, "Tomographic image reconstruction from optical projections in light-diffusing media," Appl. Opt. **36**, 180-213 (1997).
6. B. Chance, E. Anday, E. Conant, S. Nioka, S. Zhou, and H. Long, "Rapid and sensitive optical imaging of tissue functional activity, and breast," in *Advances in Optical Imaging and Photon Migration*, J. G. Fujimoto and M. S. Patterson, Eds. (Optical Society of America, Washington, DC, 1998), pp. 218-225.
7. R. Bright, "Diseases of the brain and nervous system," in *Reports of Medical Cases Selected with a View of Illustrating the Symptoms and Cure of Diseases by a Reference to Morbid Anatomy* (Longman, Rees, Orms, Brown and Green, London, 1831), Vol. II, Case CCV, p. 431.
8. T. B. Curling, "Simple hydrocele of the testis," in *A Practical Treatise on the Diseases of the Testis and of the Spermatic Cord and Scrotum* (Samuel Highley, London, 1843), pp. 125-181.
9. H. Feldmann, "[History of diaphanoscopy. Pictures from the history of otorhinolaryngology, illustrated by instruments from the collection of the Ingolstadt German Medical History Museum]," Laryngorhinootologie. **77**, 297-304 (1998).
10. M. Cutler, "Transillumination as an aid in the diagnosis of breast lesions," Surg. Gynecol. Obstet. **48**, 721-729 (1929).
11. C. Gros, Y. Quenneville, and Y. Hummel, "Diaphanologie mammaire [Breast diaphanology]," J. Radiol. Electrol. Med. Nucl. **53**, 297-306 (1972).
12. B. Ohlsson, J. Gundersen, and D.-M. Nilsson, "Diaphanography: A method for evaluation of the female breast," World J. Surg. **4**, 701-707 (1980).
13. C. H. Jones and S. P. Newbery, "Visualization of superficial vasculature using a vidicon camera tube with silicon target," Br. J. Radiol. **50**, 209-210 (1977).
14. R. F. Girolamo and J. V. Gaythorpe, "Clinical diaphanography — Its present perspective," CRC Crit. Rev. Oncol./Hematol. **2**, 1-31 (1989).
15. A. Alveryd, I. Andersson, K. Aspegren, G. Balldin, N. Bjurstam, G. Edström, G. Fagerberg, U. Glas, O. Jarlman, S. Larsson, et al., "Lightscanning versus

mammography for the detection of breast cancer in screening and clinical practice. A Swedish multicenter study," Cancer **65**, 1671-1677 (1990).

16. M. S. Patterson, B. Chance, and B. C. Wilson, "Time resolved reflectance and transmittance for the non-invasive measurement of tissue optical properties," Appl. Opt. **28**, 2331-2336 (1989).
17. R. C. Haskell, L. O. Svaasand, T.-T. Tsay, T.-C. Feng, M. S. McAdams, and B. J. Tromberg, "Boundary conditions for the diffusion equation in radiative transfer," J. Opt. Soc. Am. A **11**, 2727-2741 (1994).
18. M. A. O'Leary, D. A. Boas, B. Chance, and A. G. Yohd, "Experimental images of heterogeneous turbid media by frequency-domain diffusing-photon tomography," Opt. Lett. **20**, 426-428 (1995).
19. K. T. Moesta, S. Fantini, H. Jess, S. Totkas, M.-A. Franceschini, M. Kaschke, and P. M. Schlag, "Contrast features of breast cancer in frequency-domain laser scanning mammography," J. Biomed. Opt. **3**, 129-136 (1998).
20. H. Heusmann, J. Kölzer, and G. Mitic, "Characterization of female breasts in vivo by time resolved and spectroscopic measurements in near infrared spectroscopy," J. Biomed. Opt. **1**, 425-434 (1996).
21. S. Fantini, M. A. Franceschini, J. B. Fishkin, B. Barbieri, and E. Gratton, "Quantitative determination of the absorption spectra of chromophores in strongly scattering media: A light-emitting-diode based technique," Appl. Opt. **33**, 5204-5213 (1994).
22. M. Gerken and G. W. Faris, "Frequency-domain immersion technique for accurate optical property measurements of turbid media," Opt. Lett. **24**, 1726-1728 (1999).
23. H. Jiang, K. D. Paulsen, U. L. Osterberg, B. W. Poque, and M. S. Patterson, "Optical image reconstruction using frequency-domain data: Simulations and experiments," J. Opt. Soc. Am. A **13**, 253-266 (1996).
24. S. R. Arridge and M. Schweiger, "A gradient-based optimisation scheme for optical tomography," Opt. Express **2**, 213-226 (1998).
25. M. J. Eppstein, D. E. Dougherty, T. L. Troy, and E. M. Sevick-Muraca, "Biomedical optical tomography using dynamic parameterization and Bayesian conditioning on photon migration measurements," Appl. Opt. **38**, 2138-2150 (1999).
26. J. S. Reynolds, T. L. Troy, R. H. Mayer, A. B. Thompson, D. J. Waters, K. K. Cornell, P. W. Snyder, and E. M. Sevick Muraca, "Imaging of spontaneous canine mammary tumors using fluorescent contrast agents," Photochem. Photobiol. **70**, 87-94 (1999).
27. B. Riefke, K. Licha, and W. Semmler, "Contrast media for optical mammography," Radiologe **37**, 749-755 (1997).
28. D. A. Benaron, "Imaging cancer in vivo using optical markers in animal and human subjects, Paper 4259B-25," presented at Molecular Probes and Dyes, Photonics West, San Jose, CA (2001).
29. D. J. Bornhop, D. S. Hubbard, M. P. Houlne, C. Adair, G. E. Kiefer, B. C. Pence, and D. L. Morgan, "Fluorescent tissue site-selective lanthanide chelate, Tb-PCTMB for enhanced imaging of cancer," Anal. Chem. **71**, 2607-2615 (1999).
30. G. W. Faris and M. J. Dyer, "Upconverting chelates for biomedical diagnostics," presented at Biomedical Topical Meetings, Miami Beach, FL (April 2000).

31. M. W. Dewhirst, E. T. Ong, R. D. Braun, B. Smith, B. Klitzman, S. M. Evans, and D. Wilson, "Quantification of longitudinal tissue $pO_2$ gradients in window chamber tumours: Impact on tumour hypoxia," Br. J. Cancer **79**, 1717-1722 (1999).

32. R. Melder, H. Salehi, and R. Jain, "Interaction of activated natural killer cells with normal and tumor vessels in cranial windows in mice," Microvasc. Res. **50**, 35-44 (1995).

33. V. G. Peters, D. R. Wyman, M. S. Patterson, and G. L. Frank, "Optical properties of normal and diseased human breast tissues in the visible and near infrared," Phys. Med. Biol. **35**, 1317-1334 (1990).

34. H. Key, E. R. Davies, P. C. Jackson, and P. N. T. Wells, "Optical attenuation characteristics of breast tissues at visible and near-infrared wavelengths," Phys. Med. Biol. **36**, 579-590 (1991).

35. T. L. Troy, D. L. Page, and E. M. Sevick-Muraca, "Optical properties of normal and diseased breast tissues," in *Biomedical Optical Spectroscopy and Diagnostics*, E. Sevick-Muraca and D. Benaron, Eds. (Optical Society of America, Washington, DC, 1996), pp. 59-66.

36. B. J. Tromberg, N. Shah, R. Lanning, A. Cerussi, J. Espinoza, T. Pham, L. Svaasand, and J. Butler, "Non-invasive in vivo characterization of breast tumors using photon migration spectroscopy," Neoplasia **2**, 26-40 (2000).

37. P. Okunieff, M. Hoeckel, E. P. Dunphy, K. Schlenger, C. Knoop, and P. Vaupel, "Oxygen tension distributions are sufficient to explain the local response of human breast tumors treated with radiation alone," Int. J. Radiat. Oncol. Biol. Phys. **26**, 631-636 (1993).

38. D. M. Brizel, G. S. Sibley, L. R. Prosnitz, R. L. Scher, and M. W. Dewhirst, "Tumor hypoxia adversely affects the prognosis of carcinoma of the head and neck," Int. J. Radiat. Oncol. Biol. Phys. **38**, 285-289 (1997).

39. P. Vaupel, O. Thews, D. K. Kelleher, and M. Hoeckel, "Oxygenation of human tumors: The Mainz experience," Strahlenther Onkol. **174**, 6-12 (1998).

40. M. Holboke, B. Tromberg, X. Li, N. Shah, J. Fishkin, D. Kidney, J. Butler, B. Chance, and A. Yodh, "Three-dimensional diffuse optical mammography with ultrasound localization in a human subject," J. Biomed. Opt. **5**, 237-247 (2000).

41. J. M. Brown and A. J. Giaccia, "The unique physiology of solid tumors: Opportunities (and problems) for cancer therapy," Cancer Res. **58**, 1408-1416 (1998).

42. P. Carmeliet and R. K. Jain, "Angiogenesis in cancer and other diseases," Nature **407**, 249-257 (2000).

43. D. M. Brizel, S. Lin, J. L. Johnson, J. Brooks, M. W. Dewhirst, and C. A. Piantadosi, "The mechanisms by which hyperbaric oxygen and carbogen improve tumour oxygenation," Br. J. Cancer **72**, 1120-1124 (1995).

44. J. L. Lanzen, R. D. Braun, A. L. Ong, and M. W. Dewhirst, "Variability in blood flow and $pO_2$ in tumors in response to carbogen breathing," Int. J. Radiat. Oncol. Biol. Phys. **42**, 855-859 (1998).

45. G. Stuben, M. Stuschke, K. Knuhmann, M. R. Horsman, and H. Sack, "The effect of combined nicotinamide and carbogen treatments in human tumour xenografts: Oxygenation and tumour control studies," Radiother. Oncol. **48**, 143-148 (1998).

46. G. D. Kennovin, F. W. Flitney, and D. G. Hirst, ""Upstream" modification of vasoconstrictor responses in rat epigastric artery supplying an implanted tumour," Adv. Exp. Med. Biol. **345**, 411-416 (1994).

47. K. M. Bell, D. J. Chaplin, B. A. Poole, V. E. Prise, and G. M. Tozer, "Modification of blood flow in the HSN tumour and normal tissues of the rat by the endothelin ET(B) receptor agonist, IRL 1620," Int. J. Cancer **80**, 295-302 (1999).

48. M. W. Dewhirst, E. T. Ong, G. L. Rosner, S. W. Rehmus, S. Shan, R. D. Braun, D. M. Brizel, and T. W. Secomb, "Arteriolar oxygenation in tumour and subcutaneous arterioles: Effects of inspired air oxygen content," Br. J. Cancer Suppl. **27**, S241-S246 (1996).

49. B. M. Fenton, E. M. Lord, and S. F. Paoni, "Enhancement of tumor perfusion and oxygenation by carbogen and nicotinamide during single- and multifraction irradiation," Radiat. Res. **153**, 75-83 (2000).

50. B. Chance, personal communication (2000).

51. J. W. Severinghaus and J. F. Kelleher, "Recent developments in pulse oximetry," Anesthesiology **76**, 1018-1038 (1992).

52. J. Sinex, "Pulse oximetry: Principles and limitations," Am. J. Emerg. Med. **17**, 59-67 (1999).

53. M. A. Franceschini, V. Toronov, M. E. Filiaci, E. Gratton, and S. Fantini, "On-line optical imaging of the human brain with 160-ms temporal resolution," Opt. Express **6**, 49-57 (2000).

54. B. Chance, E. Anday, S. Nioka, S. Zhou, L. Hong, K. Worden, C. Li, T. Murray, Y. Ovetsky, D. Pidikiti, and R. Thomas, "A novel method for fast imaging of brain function, non-invasively, with light," Opt. Express **2**, 411-423 (1998).

55. D. A. Benaron, S. R. Hintz, A. Villringer, D. Boas, A. Kleinschmidt, J. Frahm, C. Hirth, H. Obrig, J. C. van Houten, E. L. Kermit, W. F. Cheong, and D. K. Stevenson, "Noninvasive functional imaging of human brain using light," J. Cereb. Blood Flow Metab. **20**, 469-477 (2000).

56. M. Tamura, Y. Hoshi, and F. Okada, "Localized near-infrared spectroscopy and functional optical imaging of brain activity," Phil. Trans. R. Soc. Lond. B Biol. Sci. **352**, 737-742 (1997).

57. S. Wray, M. Cope, D. T. Delpy, J. S. Wyatt, and E. O. R. Reynolds, "Characterization of the near infrared absorption spectra of cytochrome $aa_3$ and haemoglobin for the non-invasive monitoring of cerebral oxygenation," Biochim. Biophys. Acta **933**, 184-192 (1988).

58. X. Wu, L. Stinger, and G. W. Faris, "Determination of tissue properties by immersion in a matched scattering fluid," Proc. SPIE **2979**, 300-306 (1997).

59. S. Prahl, "Optical absorption of hemoglobin," from http://omlc.ogi.edu/spectra/hemoglobin/index.html (Oregon Medical Laser Center, 2003).

60. D. T. Delpy, M. Cope, P. van der Zee, S. Arridge, S. Wray, and J. Wyatt, "Estimation of optical pathlength through tissue from direct time of flight measurement," Phys. Med. Biol. **33**, 1433-1442 (1988).

61. J. G. Kim, D. Zhao, Y. Song, A. Constantinescu, R. P. Mason, and H. Liu, "Interplay of tumor vascular oxygenation and tumor pO2 observed using near-infrared spectroscopy, an oxygen needle electrode, and 19F MR pO2 mapping," J. Biomed. Opt. **8**, 53-62 (2003).

62. L. Sirovich and E. Kaplan, "Analysis methods for optical imaging," in *Methods for In Vivo Optical Imaging of the Central Nervous System*, R. Frostig, Ed. (CRC Press, 2001).

63. L. Sirovich and R. Everson, "Management and analysis of large scientific datasets," Intl. J. Supercomputer Applications **6**, 50-68 (1992).

64. R. M. Everson, A. K. Prashanth, M. Gabbay, B. W. Knight, L. Sirovich, and E. Kaplan, "Representation of spatial frequency and orientation in the visual cortex," Proc. Natl. Acad. Sci. U. S. A. **95**, 8334-8338 (1998).

65. P. M. Eckman and G. W. Faris, "Convolution backprojection reconstruction from photon density waves," in *OSA Trends in Optics and Photonics on Advances in Optical Imaging and Photon Migration. Vol. 2 From the Topical Meeting*, R. R. Alfano and J. G. Fujimoto, Eds. (Optical Society of America, Washington, DC, 1996), pp. 305-306.

66. E. Briggs and G. W. Faris, "Accuracy tests of frequency domain immersion technique," in *OSA TOPS Vol. 21, Advances in Optical Imaging and Photon Migration*, J. G. Fujimoto and M. S. Patterson, Eds. (Optical Society of America, Washington, DC, 1998), pp. 40-41.

67. M. Gerken and G. W. Faris, "High-accuracy optical-property measurements using a frequency domain technique," Proc. SPIE **3597**, 593-600 (1999).

68. M. Gerken and G. W. Faris, "High-precision frequency-domain measurements of the optical properties of turbid media," Opt. Lett. **24**, 930-932 (1999).

69. M. Gerken, D. Godfrey, and G. W. Faris, "Application of frequency domain techniques to samples with moderate scatter," Proc. SPIE **3599**, 86-92 (1999).

70. M. Gerken, D. Godfrey, and G. W. Faris, "Frequency-domain technique for optical property measurements in moderately scattering media," Opt. Lett. **25**, 7-9 (2000).

71. G. W. Faris, G. Alexandrakis, D. R. Busch, and M. S. Patterson, "Experimental tests of a two-layer Monte Carlo – diffusion hybrid model for photon migration in the frequency domain," Proceedings of SPIE **4250**, 313-318 (2001).

72. G. Alexandrakis, D. R. Busch, G. W. Faris, and M. S. Patterson, "Determination of the optical properties of two-layer turbid media using a frequency domain hybrid Monte Carlo diffusion model," Appl. Opt. **40**, 3810-3821 (2001).

73. C. Baltes and G. W. Faris, "Frequency domain measurements in the P3 approximation," in preparation (2003).

74. G. W. Faris and R. L. Byer, "Quantitative three-dimensional optical tomographic imaging of supersonic flows," Science **238**, 1700-1702 (1987).

75. G. W. Faris and R. L. Byer, "Beam-deflection optical tomography," Opt. Lett. **12**, 72-74 (1987).

76. G. W. Faris and R. L. Byer, "Quantitative optical tomographic imaging of a supersonic jet," Opt. Lett. **11**, 413-415 (1986).

77. G. W. Faris and H. M. Hertz, "Tunable differential interferometer for optical tomography," Appl. Opt. **28**, 4662-4667 (1989).

78. G. W. Faris and H. Bergström, "Two-wavelength beam deflection technique for electron density measurements in laser-produced plasmas," Appl. Opt. **30**, 2212-2218 (1991).

79. G. W. Faris, E. Brinkman, and J. B. Jeffries, "Density measurements in a DC arc jet using scanned beam deflection tomography," Opt. Express **7**, 447- 460 (2000).

80. G. W. Faris and R. L. Byer, "Three-dimensional beam-deflection optical tomography of a supersonic jet," Appl. Opt. **27**, 5202-5212 (1988).

81. M. A. Franceschini, S. Fantini, A. Cerussi, B. Barbieri, B. Chance, and E. Gratton, "Quantitative spectroscopic determination of hemoglobin concentration and saturation in a turbid medium: Analysis of the effect of water absorption," J. Biomed. Opt. **2**, 147-153 (1997).

82. M. Neeman, H. Dafni, O. Bukhari, R. D. Braun, and M. W. Dewhirst, "In vivo BOLD contrast MRI mapping of subcutaneous vascular function and maturation: validation by intravital microscopy," Magn. Reson. Med. **45**, 887-898 (2001).

83. X. Wu and G. W. Faris, "Compensated transillumination," Appl. Opt. **38**, 4262-4265 (1999).

84. S. Fantini, M. A. Franceschini, G. Gaida, E. Gratton, H. Jess, W. W. Mantulin, K. T. Moesta, P. M. Schlag, and M. Kaschke, "Frequency-domain optical mammography: Edge effect corrections," Med. Phys. **23**, 149-157 (1996).

85. S. Zhou, C. Xie, S. Nioka, H. Liu, Y. Zhang, and B. Chance, "Phased-array instrumentation appropriate to high-precision detection and localization of breast tumor," Proc. SPIE **2979**, 98-106 (1997).

86. H. Yu, M. Y. Su, Z. Wang, and O. Nalcioglu, "A longitudinal study of radiation-induced changes in tumor vasculature by contrast-enhanced magnetic resonance imaging," Radiat. Res. **158**, 152-158 (2002).

87. E. L. Hull, D. L. Conover, and T. H. Foster, "Carbogen-induced changes in rat mammary tumour oxygenation reported by near infrared spectroscopy," Br. J. Cancer **79**, 1709-1716 (1999).

88. R. Steen, D. Wilson, C. Bowser, J. Wehrle, J. Glickson, and S. Rajan, "$^{31}$P NMR spectroscopic and near infrared spectrophotometric studies of effects of anesthetics on in vivo RIF-1 tumors. Relationship to tumor radiosensitivity," NMR Biomed. **2**, 87-92 (1989).

89. J. G. Kim, Y. Song, D. Zhao, A. Constantinescu, R. P. Mason, and H. Liu, "Tumor oxygen dynamics by near-infrared spectroscopy, Paper 4250-75," presented at Optical Tomography and Spectroscopy of Tissue IV, Photonics West, San Jose, CA (2001).

90. Y. Gu, V. A. Bourke, J. G. Kim, A. Constantinescu, R. P. Mason, and H. Liu, "Dynamic response of breast tumor oxygenation to hyperoxic respiratory challenge monitored with three oxygen-sensitive parameters," Appl. Opt. **42**, 2960-2967 (2003).

91. D. L. Conover, B. M. Fenton, T. H. Foster, and E. L. Hull, "An evaluation of near infrared spectroscopy and cryospectrophotometry estimates of haemoglobin oxygen saturation in a rodent mammary tumour model," Phys. Med. Biol. **45**, 2685-2700 (2000).

92. R. L. Barbour, S. Zhong, H. L. Graber, Y. Pei, S.-L. S. Barbour, F. Arif, A. H. Hielscher, A. Klose, A. Bluestone, R. Andronica, and H. Luo, "Optical tomographic cinematography of vascular reactivity," presented at Optical Society of America Annual Meeting, Santa Clara, CA (1999).

93. C. H. Schmitz, H. L. Graber, H. Luo, I. Arif, J. Hira, Y. Pei, A. Bluestone, S. Zhong, R. Andronica, I. Soller, N. Ramirez, S.-L. S. Barbour, and R. L. Barbour, "Instrumentation and calibration protocol for imaging dynamic features in dense-scattering media by optical tomography," Appl. Opt. **39**, 6466-6486 (2000).

94. Y. Pei, H. L. Graber, and R. L. Barbour, "Influence of systematic errors in reference states on image quality and on stability of derived information for dc optical imaging," Appl. Opt. **40**, 5755-5769 (2001).

95. A. Bluestone, G. Abdoulaev, C. Schmitz, R. Barbour, and A. Hielscher, "Three-dimensional optical tomography of hemodynamics in the human head," Opt. Express **9**, 272-286 (2001).

96. X. Intes, J. Ripoll, Y. Chen, S. Nioka, A. G. Yodh, and B. Chance, "In vivo continuous-wave optical breast imaging enhanced with Indocyanine Green," Med. Phys. **30**, 1039-1047 (2003).

# Objectives

- Provide inexpensive technology to improve early detection of breast cancer
- Use functional optical imaging and contrast enhancement following inspiration of varying levels of carbon dioxide and oxygen
- Image various tumor types and sizes

## Vascular Function

- Angiogenesis occurs in tumors >~100 μm
- Associated tumor vasculature is often abnormal
  - Low oxygenation improvement
  - Blood pooling
  - Opposite response to different gas concentrations

# Optical Spectroscopy

- Low light absorption in IR region through tissue

  Largest components:
  - $H_2O$
  - oxyHb
  - deoxyHb

  Oxygenation levels can be determined with two wavelengths

  Optical spectroscopy reveals dynamic physiological information

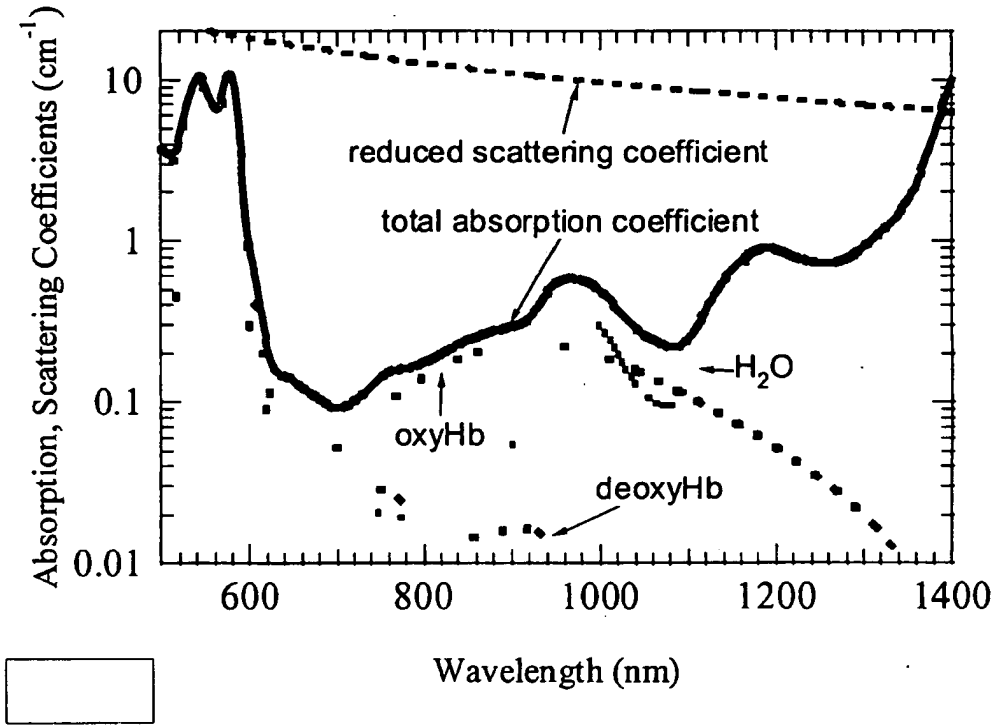

# Experimental Details

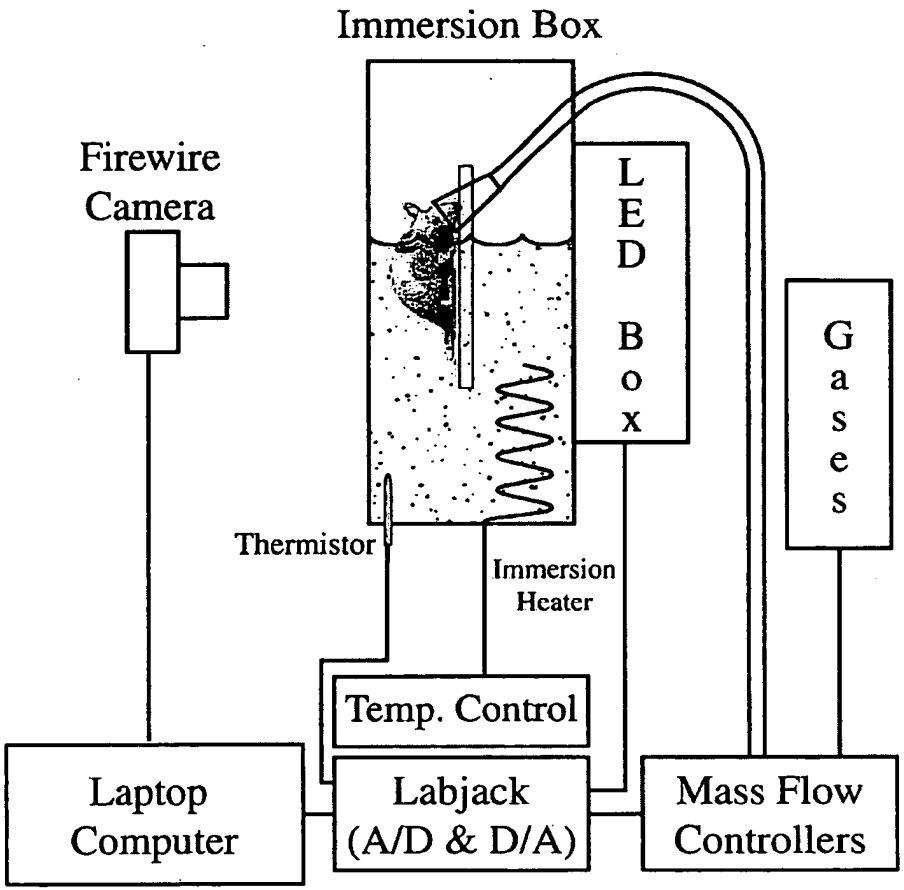


- Female athymic nude mice
- 780 nm & 840 nm LEDs
- Gases: Air, $O_2$, $CO_2$
- Imaging rate ~0.5 Hz (Upper limit ~7.5 Hz)
- Animal model allows study of contrast during tumor progression and over a range of tumor sizes

# Sample Static Images

840 nm transmission images, large U87 Brain tumor

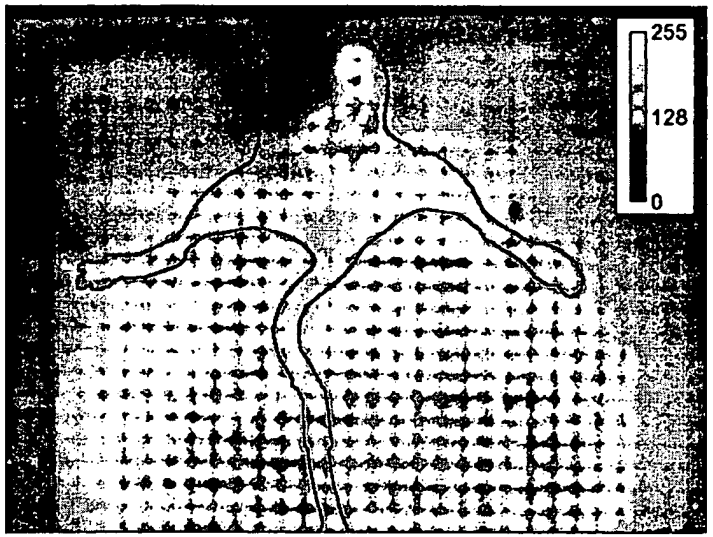


Mouse dorsal to camera

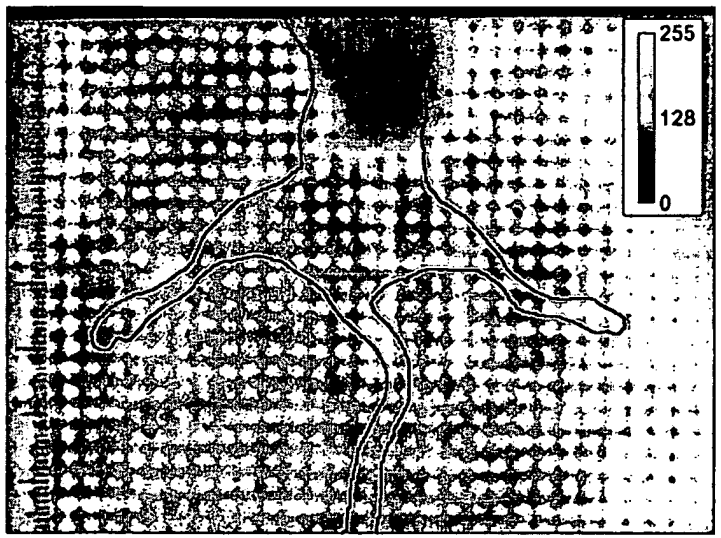


Mouse ventral to camera

# Dynamic Absorbance Images

$$\mu_a^{\lambda} = 2.3\left\{\varepsilon_{Hb}^{\lambda}[Hb] + \varepsilon_{HbO_2}^{\lambda}[HbO_2]\right\}$$

$$\Delta\mu_a^{\lambda} = \mu_a^{\lambda,t} - \mu_a^{\lambda,baseline} = 2.3\log_{10}\left[\frac{I_{baseline}}{I_t}\right]/l$$

$$\begin{pmatrix}\Delta\mu_a^{780}\\ \Delta\mu_a^{840}\end{pmatrix} = \frac{2.3}{l} * \begin{bmatrix}\varepsilon_{Hb}^{780} & \varepsilon_{Hb_{O_2}}^{780}\\ \varepsilon_{Hb}^{840} & \varepsilon_{Hb_{O_2}}^{840}\end{bmatrix}\begin{pmatrix}\Delta[Hb]\\ \Delta[HbO_2]\end{pmatrix}$$

$$\Delta[Hb](t) = \left(1.71 * \log_{10}\frac{I_{B}^{780}}{I_{t}^{780}} - 1.13 * \log_{10}\frac{I_{B}^{840}}{I_{t}^{840}}\right)/l,$$

$$\Delta[HbO_2](t) = \left(-1.20 * \log_{10}\frac{I_{B}^{780}}{I_{t}^{780}} + 1.70 * \log_{10}\frac{I_{B}^{840}}{I_{t}^{840}}\right)/l,$$

$$\Delta[Hbtot](t) = \Delta[Hb](t) + \Delta[HbO_2](t)$$

Assume Hb and $HbO_2$ are the only significant absorbers.

Calculate a time-dependent change in absorption at each wavelength by subtracting a static background image

Using the λ-dependent absorption cross-sections of Hb and $HbO_2$, we can calculate the change in concentrations of Hb, $HbO_2$ and $Hb_{total}$

# Dynamic Oxygenation Changes

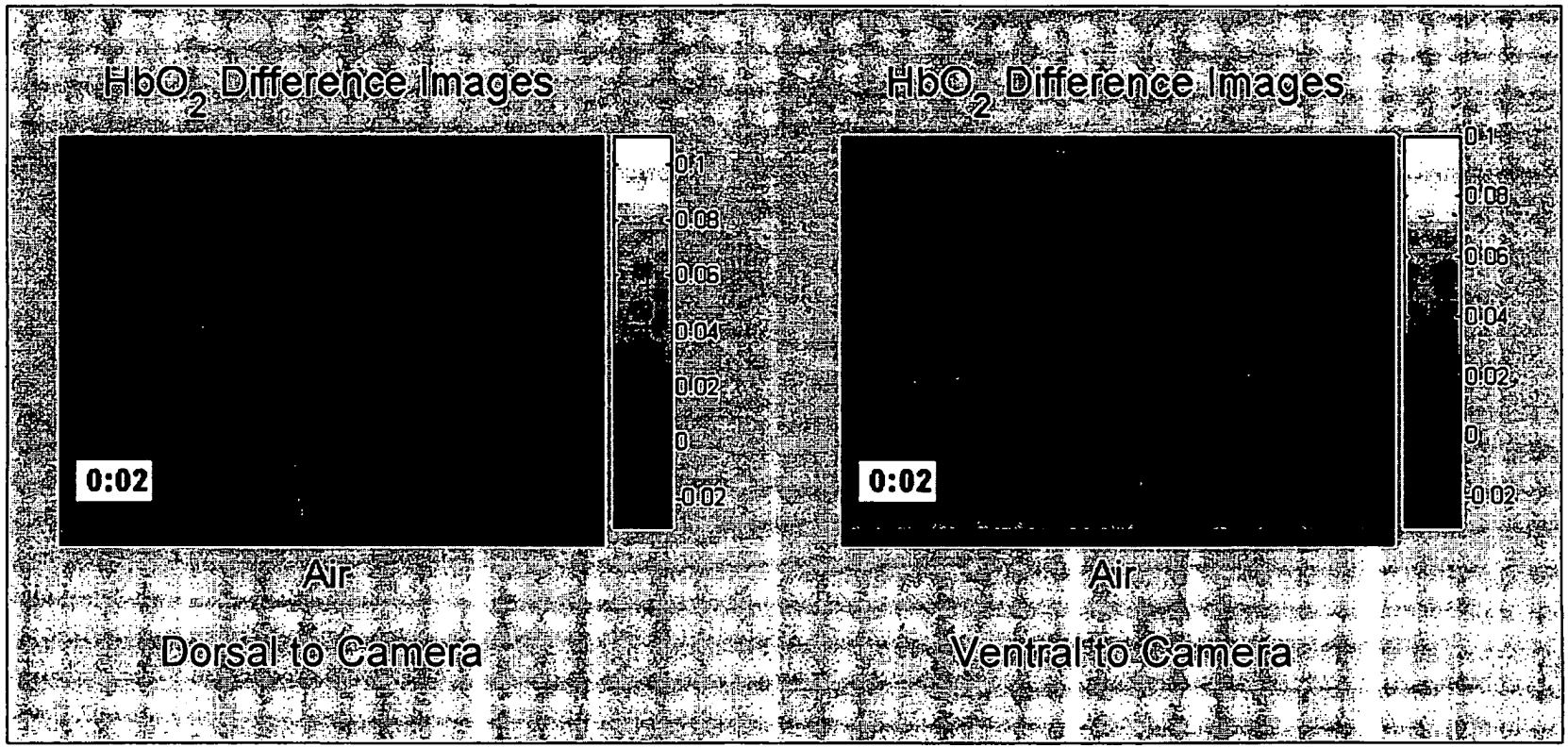

# Data Analysis & Processing

First look at the time-averaged mean and standard deviations of each pixel

Hb Mean

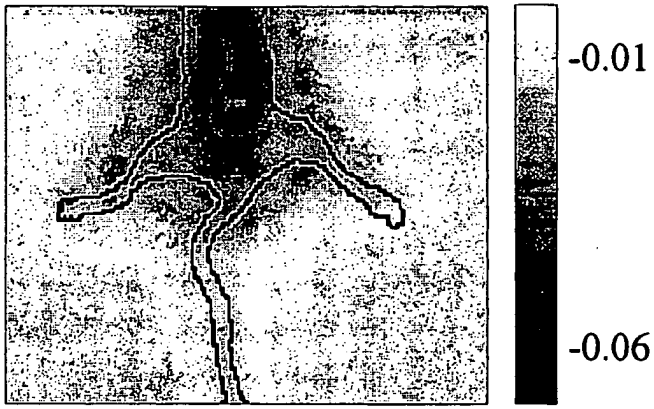


$HbO_2$ Mean

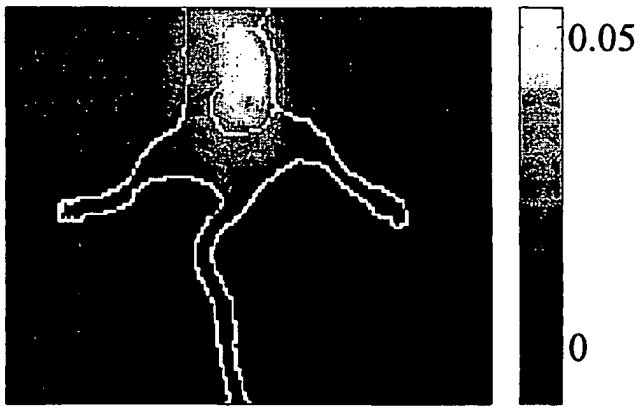


Hb Standard Deviation

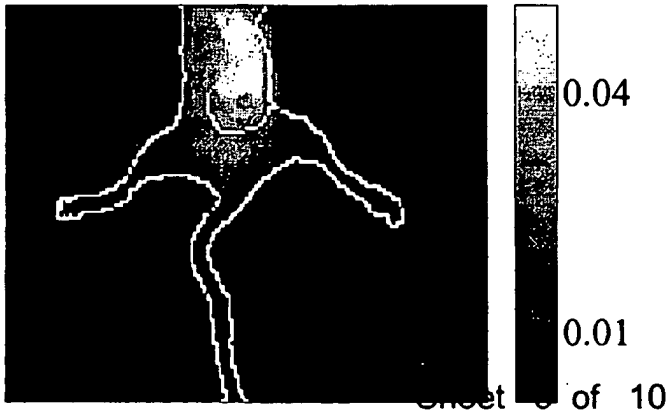


$HbO_2$ Standard Deviation

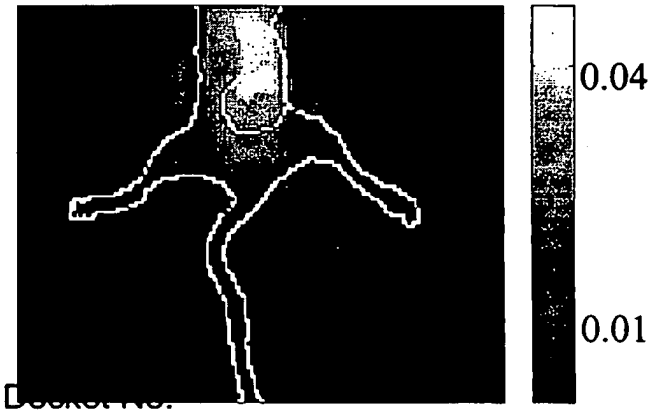

# Principle Components Analysis

Set of images can be decomposed into a orthanormal basis functions

$$f(t,\mathbf{x}) = \sum_n \mu_n a_n(t)\varphi_n(\mathbf{x}),$$

through standard matrix eigenvalue decomposition.

First Eigenimage


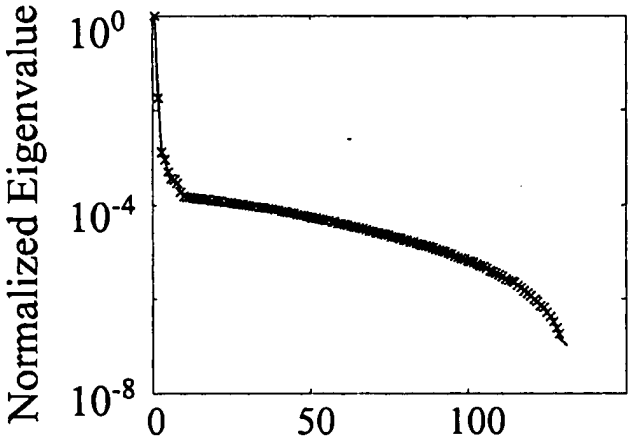


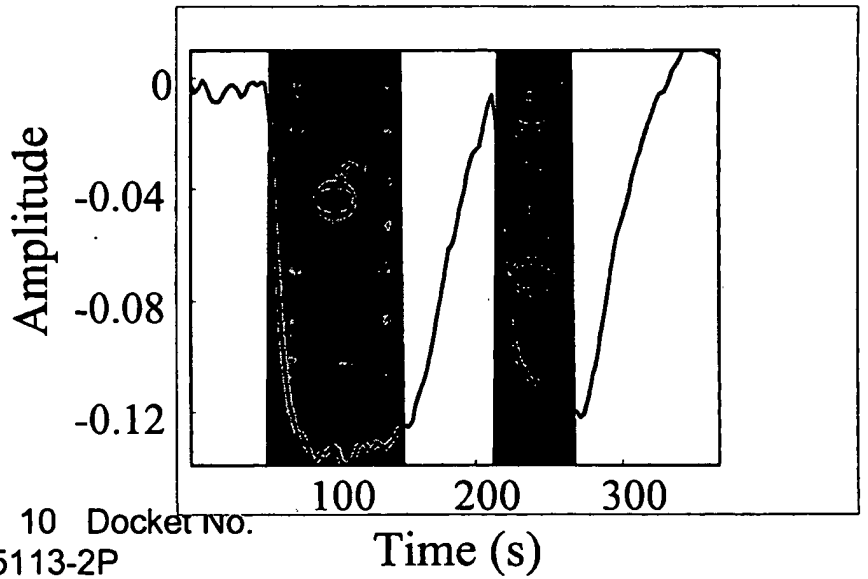

# Multiple Data Sets

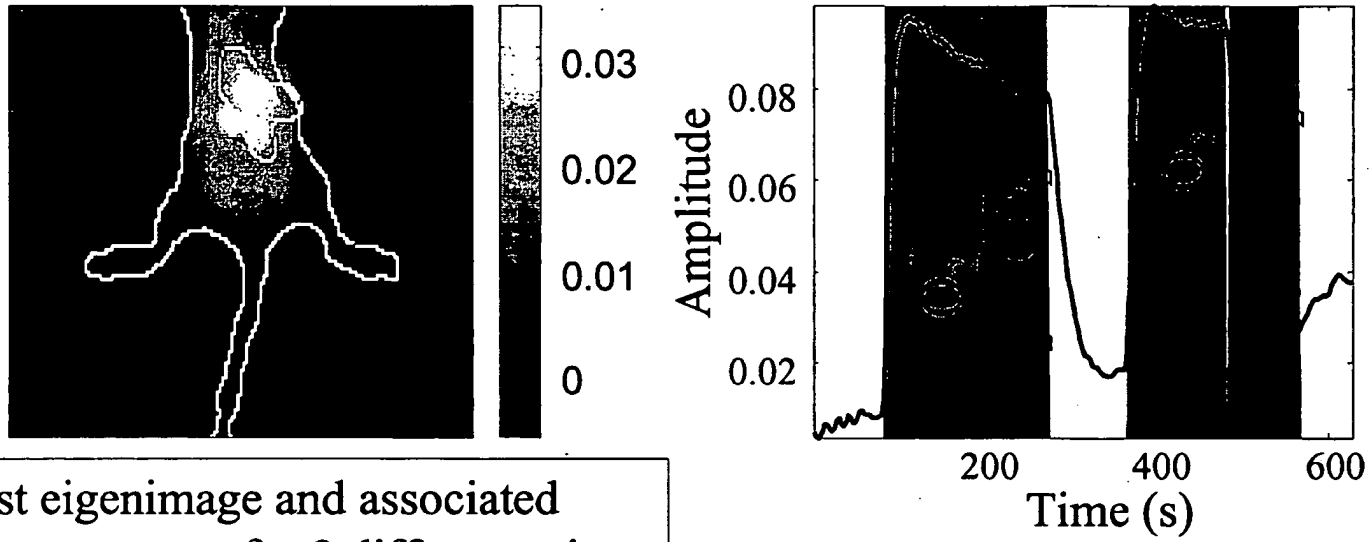


First eigenimage and associated time-responses for 2 different mice

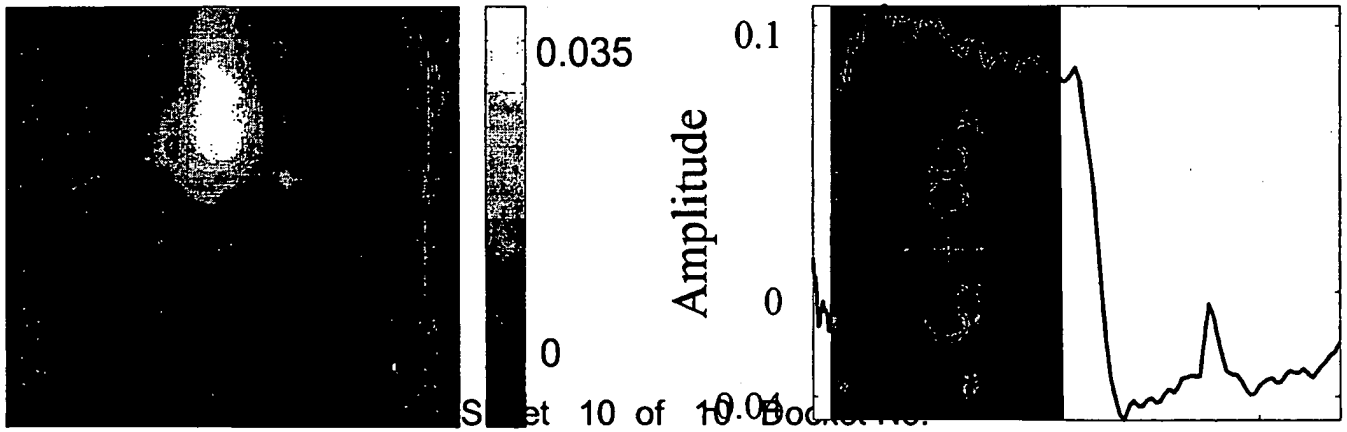

Attorney Docket No. US-5113-2P

## STATEMENT CLAIMING SMALL ENTITY STATUS
## (37 CFR 1.27(a)(3))--NONPROFIT ORGANIZATION

Applicant: SRI INTERNATIONAL
Application No.: Not Yet Known
Filed: January 23, 2004
Title: CANCEROUS TUMOR DETECTION USING OPTICAL VASCULAR FUNCTION

I hereby state that I am an official empowered to act on behalf of the nonprofit organization identified below:
NAME OF NONPROFIT ORGANIZATION: **SRI INTERNATIONAL**
ADDRESS OF NONPROFIT ORGANIZATION: **333 Ravenswood Avenue**
**Menlo Park, CA 94025**

TYPE OF NONPROFIT ORGANIZATION: UNIVERSITY OR OTHER INSTITUTION OF HIGHER EDUCATION
**TAX EXEMPT UNDER INTERNAL REVENUE SERVICE CODE (26 U.S.C. 501(a) and 501(c)(3))**

NONPROFIT SCIENTIFIC OR EDUCATIONAL UNDER STATUTE OF STATE OF THE UNITED STATES OF AMERICA
NAME OF STATE *CALIFORNIA*
CITATION OF STATUTE California Corporations Code Section 5110, et seq.

WOULD QUALIFY AS TAX EXEMPT UNDER INTERNAL REVENUE SERVICE CODE (26 U.S.C. 501(a) and 501(c)(3)) IF LOCATED IN THE UNITED STATES OF AMERICA
WOULD QUALIFY AS NONPROFIT SCIENTIFIC OR EDUCATIONAL UNDER STATUTE OF STATE OF THE UNITED STATES OF AMERICA IF LOCATED IN THE UNITED STATES OF AMERICA
(NAME OF STATE _____)
(CITATION OF STATUTE _____)

I hereby state that the nonprofit organization identified above qualifies as a nonprofit organization as defined in 37 CFR
1.27(a)(3) for purposes of paying reduced fees to the United States Patent and Trademark Office regarding the invention described
in:

[X] the specification filed herewith with title as listed above.
[ ] the application identified above.
[ ] the patent identified above.

I hereby state that rights under contract or law have been conveyed to and remain with the nonprofit organization regarding the above identified invention. If the rights held by the nonprofit organization are not exclusive, each individual, concern, or organization having rights in the invention must file separate statements as to their status as small entities and that no rights to the invention are held by any person, other than the inventor, who would not qualify as an independent inventor under 37CFR 1.27(a)(1) if that person made the invention, or by any concern which would not qualify as a small business concern under 37 CFR 1.27(a)(2) or a nonprofit organization under 37 CFR 1.27(a)(3)(i).

Each person, concern, or organization having any rights in the invention is listed below:

[X] no such person, concern, or organization exists.
[ ] each such person, concern, or organization is listed below.

I acknowledge the duty to file, in this application or patent, notification of any change in status resulting in loss of entitlement to small entity status prior to paying, or at the time of paying, the earliest of the issue fee or any maintenance fee due after the date on which status as a small entity is no longer appropriate. (37 CFR 1.27(g))

NAME OF PERSON SIGNING Edward E. Davis
TITLE IN ORGANIZATION OF PERSON SIGNING Assistant S cretary
ADDRESS OF PERSON SIGNING: SRI International, 333 Ravenswood Avenue, Menlo Park, CA 94025

SIGNATURE  DATE January 23, 2004